Precambrian Research 270 (2015) 246–266

Contents lists available at ScienceDirect

Precambrian Research

journal homepage: www.elsevier.com/locate/precamres

Episodic Paleoarchean-Paleoproterozoic (3.3–2.0 Ga) granitoid magmatism in Yangtze Craton, South China: Implications for late Archean tectonics

Jing-Liang Guo*, Yuan-Bao Wu, Shan Gao, Zhen-Min Jin, Ke-Qing Zong, Zhao-Chu Hu, Kang Chen, Hai-Hong Chen, Yong-Sheng Liu

State Key Laboratory of Geological Processes and Mineral Resources, School of Earth Sciences, China University of Geosciences, 430074 Wuhan, China

ARTICLE INFO

Article history:
Received 26 April 2015
Received in revised form 9 August 2015
Accepted 4 September 2015
Available online 10 September 2015

Keywords:
Archean
Continental crust
TTG
Plate tectonics
Supercontinent
Yangtze Craton

ABSTRACT

The Archean Kongling Terrane preserves voluminous Paleoarchean-Paleoproterozoic granitoids, recording the early formation and evolution history of the Yangtze Craton, South China. We present petrography, geochemistry, zircon U–Pb geochronology and Lu–Hf isotopes of twelve gneissic granitoids from this terrane, including trondhjemites, biotite-granites, and two-mica granites. Magmatic zircons in these granitoids yield emplacement ages of 3.31–3.29 Ga for trondhjemites, 2.81–2.78 and 2.66 Ga for biotite-granites, as well as 2.70–2.64, 2.42, and 2.00 Ga for two-mica granites. The 2.8–2.6 Ga granites contain minor 3.4–2.9 Ga inherited zircons and 2.0 Ga metamorphic zircons that formed mainly by recrystallization. Major and trace element compositions of the trondhjemites suggest a garnet amphibolite-facies low-K mafic source, similar to the typical Archean medium-pressure trondhjemite-tonalite-granodiorites (TTGs), whereas those of the biotite- and two-mica granites indicate tonalitic and tonalitic-sedimentary sources, respectively. The Lu–Hf data (chondritic $\varepsilon_{Hf}(t)$ values −0.8 to 0 and Eoarchean two-stage Hf model ages 3.75–3.70 Ga) for the trondhjemites support partial melting of a long-lived ancient depleted-mantle-derived or a juvenile lower-mantle-derived mafic crust. The Lu–Hf data and inherited zircon ages also suggest that the 2.8 Ga granites were derived from the local 3.4–2.9 Ga TTGs. Together with previously addressed 3.2 and 3.0–2.9 Ga TTG magmatism, a remarkable change is observed at 2.8 Ga in the petrology, geochemistry, and petrogenesis of the episodic 3.3–2.0 Ga granitoid magmatism from TTG- to granite-dominated in the Kongling Terrane, which may reflect a transition from subduction- to collision-related tectonics. In addition, we note that the 2.70–2.64 Ga biotite- and two-mica granites (this study) as well as 2.67–2.62 Ga A-type granites (published data) were emplaced shortly after a 2.75–2.72 Ga high-grade metamorphic event (published data) in the Kongling Terrane. These granites could be generated as a result of orogenic root collapse and subsequent mantle upwelling, implying a 2.7 Ga orogenic event in the Yangtze Craton.

1. Introduction

Archean Era is one of the most important periods for the formation of the continental crust (Armstrong and Harmon, 1981; Taylor and McLennan, 1985; Collerson and Kamber, 1999; Belousova et al., 2010; Hawkesworth et al., 2010, 2013; Wang et al., 2011; Dhuime et al., 2012; Condie, 2014). Different from the post-Archean continental crusts, the Archean crusts have several unique features. Firstly, the Archean crusts are featured by high-grade metamorphic terranes dominated by pervasively deformed tonalite-trondhjemite-granodiorites (TTGs), whereas the post-Archean crusts are usually dominated by granites (Taylor and McLennan, 1985; Martin, 1993, 1994; Nutman et al., 1996; Moyen, 2011; Kröner et al., 2014; Laurent et al., 2014). Secondly, the early Archean crusts apparently lack 'hallmarks' of modern-style plate tectonics (e.g., ophiolites, eclogites, and ultra-high pressure metamorphism), implying different geodynamics from the post-Archean (Bradley, 2008, 2011; Shirey and Richardson, 2011). Thirdly, the Archean crusts have much higher geothermal gradients, resulting in special rock types (e.g., komatiites) and distinct geodynamics from the post-Archean ones (e.g., stagnant-lid vs. plate tectonics) (Martin, 1993; Wilson et al., 2003; Ernst, 2009;

* Corresponding author at: School of Earth Sciences, China University of Geosciences, Lumo Road 388, 430074 Wuhan, China. Tel.: +86 (0)27 6788 3001; fax: +86 (0)27 6788 3001.
E-mail address: jl.guo@cug.edu.cn (J.-L. Guo).

http://dx.doi.org/10.1016/j.precamres.2015.09.007
0301-9268/

Johnson et al., 2014; Rey et al., 2014). Moreover, the formation and evolution of the Archean crust played a key role in the advent of a habitable climate and life (e.g., Schopf, 1993; Mojzsis et al., 1996; Furnes et al., 2004; Campbell and Allen, 2008; McLoughlin et al., 2012; Staudigel et al., 2015). Such unique nature of the Archean continental crust makes it special in Earth's history.

The high-grade metamorphic terranes that feature the Archean crusts are mainly composed of granitoids, which can be classified into four groups (cf., Moyen et al., 2003; Laurent et al., 2014): (1) volumetrically-dominant and juvenile TTGs, whose geochemistry is consistent with an origin through partial melting of meta-igneous mafic rocks at various pressures; (2) Mg-, Fe- and K-rich, metaluminous (monzo)diorites and granodiorites, referred to as sanukitoids s.l., which were derived primarily from hybridization between mantle peridotite and a component rich in incompatible elements; (3) peraluminous and K-rich biotite- and two-mica granites, formed through melting of older crustal lithologies (TTGs and metasediments, respectively); and (4) hybrid high-K granites with mixed characteristics from the former three groups. Previous studies have shown that the general pattern of emplacement age, lithology, and petrogenesis of these granitoid rocks is of great significance, for instance, in constraining the growth and differentiation of continental crust (Jahn et al., 2000; Kemp et al., 2006, 2007; Condie et al., 2009), the onset of modern-style plate tectonics in a global scale (Laurent et al., 2014), and the reconstruction of Archean supercontinent or supercraton (Condie et al., 2009; Condie and Aster, 2010; Pehrsson et al., 2013). This general pattern can be only addressed by using a combination of field work, whole-rock petrography and geochemistry, precise dating and isotope techniques on granitoid samples from a series of Archean terranes (e.g., Zeh et al., 2009, 2010; Laurent et al., 2013; Kröner et al., 2014).

The Yangtze Craton and the North China Craton are the two most important Archean cratons in eastern Asia, both of which were originated before 3.8 Ga (Liu et al., 1992; Song et al., 1996; Wan et al., 2005, 2012; Zhang et al., 2006c; Gao et al., 2011; Guo et al., 2014b). Compared to the North China Craton, where the Archean rocks are widely distributed (Zhai and Santosh, 2011; Zhao and Cawood, 2012; Zhao and Zhai, 2013), the Yangtze Craton has very limited exposure of the Archean basement that primarily outcrops in the northern part of the Kongling Terrane (Gao and Zhang, 1990; Gao et al., 1999; Zhao and Cawood, 2012). Unlike the well studied Superior, Kaapvaal, and North China Cratons, the early formation and evolution pattern of the Yangtze Craton has not been well constrained.

Here, we report the whole-rock geochemistry, zircon U–Pb geochronology and Lu–Hf isotopes of twelve gneissic granitoids from the Kongling Terrane in the Yangtze Craton, South China. U–Pb data reveal that these granitoids were emplaced at 3.3, 2.8, 2.7–2.6, 2.4, and 2.0 Ga, respectively. Combined with previously published data, the granitoid magmatism in the Kongling Terrane exhibits a crucial change in petrology (from TTG- to granite-dominated), geochemistry (from Na- to K-rich), and petrogenesis (from mafic to felsic sources) at 2.8 Ga. This transition may play an important role in the cratonization and differentiation of the Yangtze Craton, and might be important for understanding the Neoarchean tectonics. In addition, we propose a 2.7 Ga orogenic event in the Yangtze Craton, which might be related to the earliest global supercontinental event.

2. Geological background

The Yangtze Craton is situated in the northwest of South China (Fig. 1a). It amalgamated with the Cathaysia Block to the south during the Neoproterozoic (Li et al., 2009), and with the North China Craton to the north during the Triassic (Liou et al., 2009; Zhang et al., 2009; Wu and Zheng, 2013) (Fig. 1a). The Archean rocks in South China are largely exposed in the Kongling Terrane (3.4–2.6 Ga) from the northern Yangtze Craton (e.g., Gao and Zhang, 1990; Gao et al., 1999, 2011; Qiu et al., 2000; Jiao et al., 2009; Chen et al., 2013; Guo et al., 2014b). Although limitedly exposed, the lateral extension of Archean crust under the sedimentary cover in the Yangtze Craton is suggested by (1) the occurrences of several small Archean outcrops in the northern Yangtze Craton, such as the 2.7 Ga Huangtuling granulites in the eastern Dabie Orogen (Wu et al., 2008), 2.65 Ga A-type granites in the Huji area (Z.J. Wang et al., 2013a, 2013b), 2.7 Ga Yudongzi Group in the South Qinling Orogen (Zhang et al., 2001), and 2.5 Ga TTGs in the Douling Complex (Hu et al., 2013; Wu et al., 2014) (Fig. 1a), (2) the U–Pb ages (2.9–2.5 Ga) and Hf model ages (3.5–2.6 Ga) of xenocryst zircons in lamproite diatremes from three Proterozoic areas in the central Yangtze Craton (Zheng et al., 2006), and (3) a recent geophysical study based on a 400-km-long high-resolution seismic reflection profile across the central-southeastern Yangtze Craton, which revealed a lateral extended crystalline basement buried by Neoproterozoic flysch strata (Dong et al., 2015).

The Kongling Terrane has long been the focus for studies of the origin and early evolution of the Yangtze Craton (e.g., Gao and Zhang, 1990; Gao et al., 1999, 2011; Qiu et al., 2000; Zhang et al., 2006a, b, c; Zheng et al., 2006; Jiao et al., 2009; Chen et al., 2013; Guo et al., 2014b). It exhibits a dome structure that covers about 360 km^2 in area (Fig. 1b). In terms of lithology and rock ages, the Kongling Terrane can be divided into two segments: (1) the North Kongling Terrane, which chiefly consists of Archean grey gneisses (e.g., TTGs and granites) and meta-sedimentary rocks (e.g., Gao and Zhang, 1990; Gao et al., 1999), and (2) the South Kongling Terrane, which is represented by the Neoproterozoic Huangling Igneous Complex that intruded into the Archean basement (e.g., Ling et al., 2006; Zhang et al., 2008; Zhao et al., 2013).

The North Kongling Terrane comprises three major rock associations, including (1) intermediate-felsic gneisses (e.g., diorites, TTGs, and granites), (2) metasedimentary rocks (e.g., metapelites and marbles), and (3) amphibolites plus locally preserved mafic granulites (Gao and Zhang, 1990; Gao et al., 1999) (Fig. 1c). The proportions of orthogneisses, clastic metasedimentary rocks, and amphibolites are about 0.51, 0.44, and 0.05, respectively (Gao et al., 1999). Early studies mainly focused on the 3.0–2.9 Ga TTG gneisses from the western North Kongling Terrane (Gao and Zhang, 1990; Qiu et al., 2000; Zhang et al., 2006a; Zheng et al., 2006; Gao et al., 2011). These rocks host minor 3.0 Ga mafic magmatic enclaves and 2.95–2.90 Ga dykes, and multiple metamorphic events (2.87, 2.73, 2.56, and 2.0 Ga) were recognized in these mafic rocks (Wei and Wang, 2012; Wei and Jing, 2013; Li et al., 2014). In the eastern North Kongling Terrane (Fig. 1c), Chen et al. (2013) reported 2.67–2.62 Ga A-type (ferroan) granites with abundant zircons of positive $\varepsilon_{Hf}(t)$ values (up to the coeval depleted-mantle value). Rare 3.4–3.2 Ga granitoid gneisses have been recently reported from the North Kongling Terrane, including 3.45 Ga granites (Guo et al., 2014b), 3.30–3.26 Ga TTGs (Gao et al., 2011), and 3.22 Ga orthogneisses (Jiao et al., 2009), which are the oldest rocks identified so far in South China (Fig. 1c). Zircon Hf isotopic data indicate that these rocks may be partial melts of ancient crust that derived from the depleted mantle at 4.0–3.6 Ga (Jiao et al., 2009; Gao et al., 2011; Guo et al., 2014b).

The Archean basement of the North Kongling Terrane was pervasively metamorphosed to amphibolite facies or high-pressure granulite facies at 2.0 Ga (Zhang et al., 2006a, b; Wu et al., 2009; Gao et al., 2011; Chen et al., 2013; Yin et al., 2013; Guo et al., 2014b), as a result of continental collision during the assembly of supercontinent Columbia (Zhao et al., 2002; Zhang et al., 2006b; Wu et al., 2009; Yin et al., 2013; Li et al., 2014). The widespread 2.0 Ga, syn-collisional S-type granites and migmatites in the Kongling Terrane

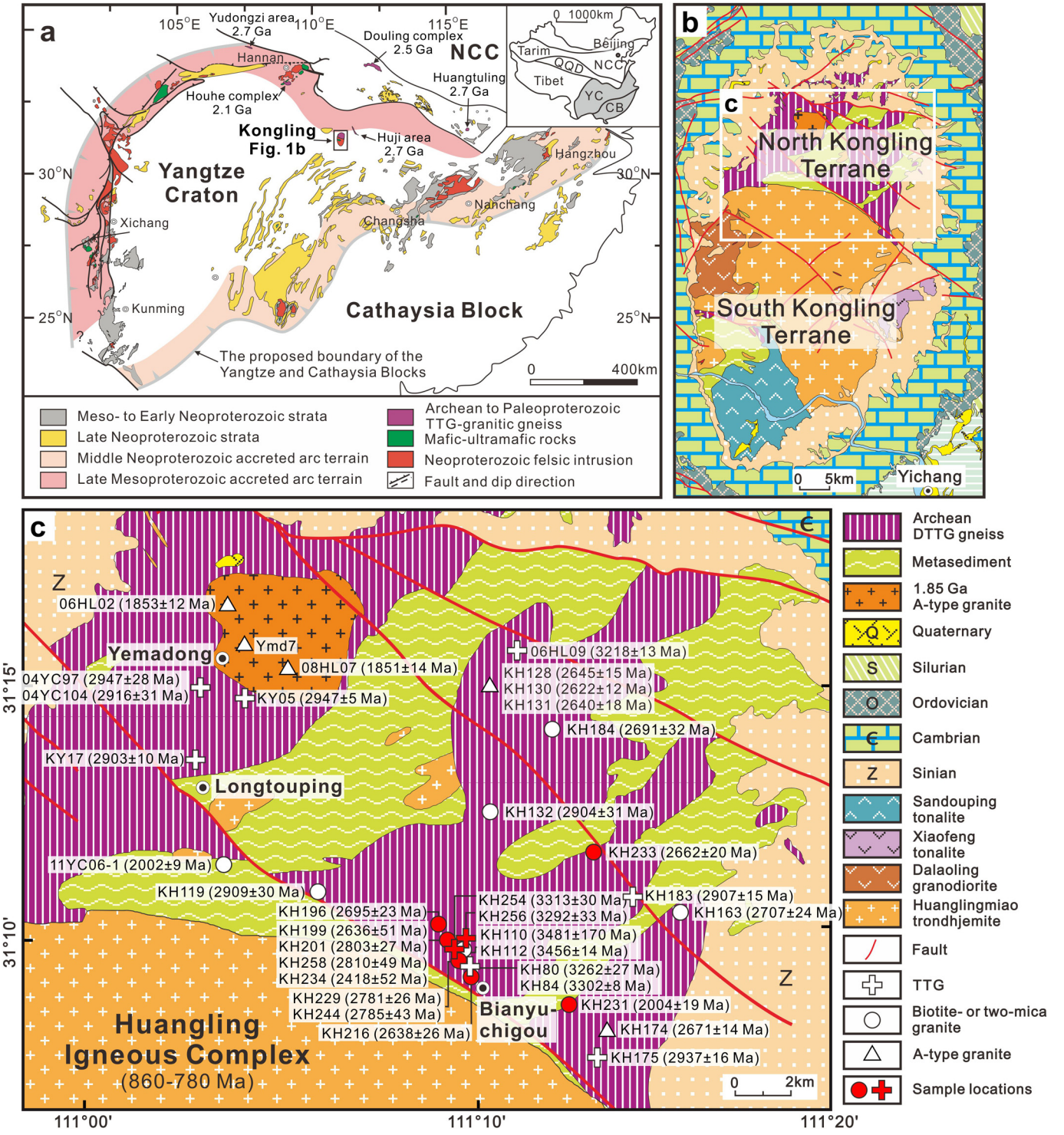

Fig. 1. (a) Distribution of Archean-Proterozoic rocks in the Yangtze Craton (modified from Zhao and Cawood, 2012). (b) Structure and division of the Kongling Terrane (modified from Gao et al., 2011). (c) Geological map of the North Kongling Terrane. Symbols: diamonds, tonalite-trondhjemite-granodiorites (TTGs); circles, biotite- or two-mica granites; triangles, A-type granites. The filled and open symbols indicate granitoid rocks from this and previous studies, respectively (Qiu et al., 2000; Zhang et al., 2006a; Jiao et al., 2009; Xiong et al., 2009; Gao et al., 2011; Peng et al., 2012; Chen et al., 2013; Yin et al., 2013; Guo et al., 2014b; Li et al., 2014). The numbers represent emplacement ages of the granitoid rocks with 2σ errors. *Abbreviations*: NCC, North China Craton; QQD, Qilian-Qinling-Dabie HP-UHP orogenic belt; YC, Yangtze Craton; CB, Cathaysia Block; DTTG, dioritic, tonalitic, trondhjemitic, and granitic.

were also attributed to this event (Yin et al., 2013; Li et al., 2014). Later, the eastern part of the North Kongling Terrane was intruded by 1.85 Ga A-type granites (Fig. 1c) and 1.85–1.78 Ga mafic dykes in an extensional tectonic setting, which marks the final cratonization of the Yangtze Craton (Peng et al., 2009, 2012; Xiong et al., 2009; Li et al., 2014).

This study investigated twelve gneissic granitoids from the Bianyuchigou area in the central North Kongling Terrane. This area is covered by thick vegetation, while the freshest rock samples were collected from this region. These samples are strongly to weakly deformed (Supplementary figure* S1). Their mineral assemblages are summarized in Table 1.

Table 1
Rock types and mineral assemblages of gneissic granitoids from the Kongling Terrane.

Sample	Rock type	Intrusion age ($\pm 2\sigma$)[a]	Mineral assemblage	Accessory minerals	GPS coordinates
KH254	Trondhjemite	3313 ± 30 Ma (n = 20)	50% Pl + 5% Kfs + 44% Qz + 1% Bi	Zrn, Ttn, Mag	31.1604°N, 111.1590°E
KH256	Trondhjemite	3292 ± 33 Ma (n = 17)	45% Pl + 10% Kfs + 35% Qz + 10% Bi	Zrn, Ttn, Mag, Ilm, Ap, Chl	31.1594°N, 111.1615°E
KH258	Biotite-granite	2810 ± 49 Ma (n = 14)	15% Pl + 35% Kfs + 47% Qz + 3% Bi	Zrn, Ttn, Mag	31.1610°N, 111.1596°E
KH201	Biotite-granite	2801 ± 27 Ma (n = 19)	30% Pl + 25% Kfs + 40% Qz + 5% Bi	Zrn, Ttn, Mag, Ilm, Gth	31.1608°N, 111.1586°E
KH244	Biotite-granite	2785 ± 43 Ma (n = 4)	25% Pl + 40% Kfs + 34% Qz + 1% Bi	Zrn, Ttn	31.1613°N, 111.1578°E
KH229	Biotite-granite	2781 ± 26 Ma (n = 11)	25% Pl + 30% Kfs + 42% Qz + 3% Bi	Zrn, Ttn, Chl	31.1583°N, 111.1586°E
KH196	Two-mica granite	2695 ± 23 Ma (n = 30)	20% Pl + 35% Kfs + 43% Qz + 1% Bi + 1% Ms	Zrn, Mag, Chl	31.1658°N, 111.1497°E
KH233	Biotite-granite	2662 ± 20 Ma (n = 33)	20% Pl + 40% Kfs + 39% Qz + 1% Bi	Zrn, Ttn	31.1856°N, 111.2222°E
KH216	Two-mica granite	2638 ± 26 Ma (n = 2)	15% Pl + 35% Kfs + 50% Qz + trace Bi and Ms	Zrn, Ttn, Mag	31.1558°N, 111.1628°E
KH199	Two-mica granite	2636 ± 51 Ma (n = 18)	15% Pl + 55% Kfs + 26% Qz + 3% Bi + 1% Ms	Zrn, Ttn, Mag, Gth	31.1625°N, 111.1547°E
KH234	Two-mica granite	2418 ± 52 Ma (n = 5)	20% Pl + 35% Kfs + 41% Qz + 3% Bi + 1% Ms	Zrn, Mag	31.1629°N, 111.1532°E
KH231	Two-mica granite	2004 ± 19 Ma (n = 16)	5% Pl + 45% Kfs + 48% Qz + 1% Bi + 1% Ms	Zrn, Ttn, Ap, Chl	31.1481°N, 111.2106°E

Pl, plagioclase; Kfs, K-feldspar; Qz, quartz; Bi, Biotite; Ms, muscovite; Zrn, zircon; Ttn, titanite; Mag, magnetite; Ilm, ilmenite; Ap, apatite; Chl, chlorite; Gth, goethite.
[a] The intrusion ages are upper intercept ages of magmatic zircons in each sample, except for KH216, which is a weighted mean $^{207}Pb/^{206}Pb$ age.

3. Analytical methods

3.1. Whole-rock major and trace element analyses

The rock samples were crushed in a corundum jaw crusher and then powdered down to <200 mesh in a tungsten carbide mill at a rotating speed of 700 rev/min. Major oxides were analyzed by XRF (Rikagu RIX 2100) using fused glass disks at the State Key Laboratory of Continental Dynamics, Northwest University, Xi'an, China. Analyses of USGS basalt and andesite standards (BCR-2, BHVO-1 and AGV-1) indicate precision and accuracy better than 5% for major elements (Rudnick et al., 2004). Trace elements were analyzed by Agilent 7500a inductively coupled plasma mass spectrometry (ICP-MS) with shielded torch at the State Key Laboratory of Geological Processes and Mineral Resources, China University of Geosciences, Wuhan. Sample powders were digested by HF + HNO_3 acid in Teflon bombs under high pressures (7–9 MPa). For most trace elements, our measured concentrations of BCR-2, BHVO-1, and AGV-1 agree with their reference values from GeoReM (http://georem.mpch-mainz.gwdg.de/) within 5% difference. Three samples were analyzed twice in order to test the analytical reproducibility, which is better than 5% for most elements. Two different batches of rock powders of one coarse-grained sample (KH231) were analyzed to evaluate the geochemical heterogeneity within one sample, which is better than 10% for most elements.

3.2. Zircon U–Pb and Lu–Hf isotope analyses

Zircon grains were separated from each sample by conventional magnetic and heavy liquid methods. They were selected and mounted on a double-sided adhesive tape, and then cast in epoxy resin in a 1-cm-diameter mount. The mount was polished to expose the center of zircons, and was cleaned by dilute HNO_3 and pure ethanol before analysis, in order to avoid surface Pb contamination. All analytical works on zircons were carried out at the State Key Laboratory of Geological Processes and Mineral Resources, China University of Geosciences, Wuhan.

3.2.1. Cathodoluminescence imaging

Cathodoluminescence (CL) images were used to reveal the internal structures of zircons, in order to determine their origins (e.g., magmatic or metamorphic) and help to select optimum spot locations for later isotope analyses. The images were acquired on a FEI Quanta 450 field emission gun (FEG) scanning electron microscope (SEM) coupled with a Gatan Mono CL4+ CL system. For zircon CL imaging, the working conditions were set to be 10 kV. The spot size was 5 μm and working distance was 14 mm.

3.2.2. LA-ICP-MS U–Pb isotope analyses

Zircon U–Pb dating was performed on a 193 nm excimer ArF laser ablation system (GeoLas 2005, Lambda Physik) coupled with an Agilent 7500a ICP-MS. The laser beam was set to 32 μm at a frequency of 6 Hz. The energy density was ~4 J/cm^2. Helium was used as carrier gas to provide efficient aerosol transport to the ICP and minimize aerosol deposition around the ablation site and within the transport tube (Eggins et al., 1998; Jackson et al., 2004). The carrier and make-up gas flows were optimized by monitoring the ^{238}U intensity during ablating NIST610. In order to enhance the sensitivity of U, Th, and Pb isotopes, 2–4 mL/min of nitrogen was added to the central gas flow (Hu et al., 2008). A novel "wire" signal smoothing device was applied to improve the signal stability (Hu et al., 2012). Each analysis incorporated a 20–30 s background acquisition, followed by a 50 s data acquisition of zircon samples. Standard zircon 91500 (Wiedenbeck et al., 1995) was employed as an external standard to calibrate isotope fractionation, which was analyzed twice for every five analyses. Standard zircons GJ-1 and FC1 were analyzed as unknowns. An in-house Excel-based software ICPMS-DataCal (v. 9.2) was used for U–Pb data reduction (Y.S. Liu et al., 2008). Detailed operating conditions for the LA-ICP-MS, analytical procedures, and data processing are similar to those described by Liu et al. (2010) and Guo et al. (2014a). Common Pb correction was applied following the method of Andersen (2002). The correction was negligible in most cases. Weighted mean and intercept ages were calculated using ISOPLOT (v. 3.76) (Ludwig, 2012). Our measurements of GJ-1 yielded a weighted mean $^{206}Pb/^{238}U$ age of 601 ± 5 Ma (1SD, n = 144), which is statistically identical to its TIMS $^{206}Pb/^{238}U$ age of 599.8 ± 1.7 Ma (2σ) (Jackson et al., 2004) (Supplementary Table S1). Measurements of FC1 yielded a weighted mean $^{207}Pb/^{206}U$ and a $^{207}Pb/^{235}U$ age of 1104 ± 21 and 1100 ± 15 Ma (1SD, n = 25), respectively, which agree with its TIMS $^{207}Pb/^{206}U$ age of 1099.0 ± 0.6 Ma (2σ) (Paces and Miller, 1993) (Supplementary Table S1).

3.2.3. LA-MC-ICP-MS Lu–Hf isotope analyses

Zircon Lu–Hf isotope analysis was conducted on a GeoLas 2005 laser ablation system connected to a Neptune Plus multiple-collector (MC) ICP-MS (Thermo Fisher Scientific). The laser was set to a spot size of 44 μm, a repetition rate of 10 Hz, and an energy density of ~4 J/cm^2. Helium was used as carrier gas. The combination of a newly designed X skimmer cone with a jet sample cone (Hu et al., 2012) was applied to the MC-ICP-MS. In order to increase the sensitivity of Hf and suppress the non-linear mass fractionation, 4–10 mL/min of nitrogen was added to the central gas flow in LA-MC-ICP-MS (Hu et al., 2012). The analyzed isotopes include ^{171}Yb, ^{173}Yb, ^{174}(Hf + Yb), ^{175}Lu, ^{176}(Hf + Yb + Lu), ^{177}Hf, ^{179}Hf, ^{180}(Hf + W), ^{182}W. The mass fractionation of Yb (β_{Yb}) was directly obtained

from the zircon sample itself in real-time. The $^{179}Hf/^{177}Hf$ and $^{173}Yb/^{171}Yb$ ratios were used to calculate the mass bias of Hf (β_{Hf}) and Yb (β_{Yb}), which were normalized to $^{179}Hf/^{177}Hf = 0.7325$ (Patchett and Tatsumoto, 1980) and $^{173}Yb/^{171}Yb = 1.1265$ (Thirlwall and Anczkiewicz, 2004), using an exponential correction for mass bias. Interference of ^{176}Yb on ^{176}Hf was corrected by measuring the interference-free ^{173}Yb isotope and using $^{176}Yb/^{173}Yb = 0.78696$ (Thirlwall and Anczkiewicz, 2004) to calculate $^{176}Yb/^{177}Hf$. Similarly, the relatively minor interference of ^{176}Lu on ^{176}Hf was corrected by measuring the intensity of the interference-free ^{175}Lu isotope and using the recommended $^{176}Lu/^{175}Lu = 0.02656$ (Blichert-Toft et al., 1997) to calculate $^{176}Lu/^{177}Hf$. The mass bias of Yb (β_{Yb}) was used to calculate the mass fractionation of Lu. Detailed procedures were described by Liu et al. (2010) and Hu et al. (2012). Time-drift correction was performed using standard zircon 91500. The interference and mass fractionation-corrected $^{176}Hf/^{177}Hf$ ratios of the samples were then calibrated against 91500 using the recommended $^{176}Hf/^{177}Hf$ ratio of 0.282308 ± 6 (2σ) (Blichert-Toft, 2008). The uncertainty of the preferred value for 91500 was propagated to the ultimate results for the samples. Data reduction was performed by ICPMSDataCal (v. 9.2) (Y.S. Liu et al., 2008). Our measured $^{176}Hf/^{177}Hf$ ratios of standard zircons R33, FC1, MunZirc (synthetic; Fisher et al., 2011), and GJ-1 are listed in Supplementary Table S2, which agree well with their reference values (Fisher et al., 2014 and references therein).

For calculating the initial $^{176}Hf/^{177}Hf$ ratios, the decay constant of 1.867×10^{-5} Ma^{-1} was used for ^{176}Lu (Söderlund et al., 2004). The $\varepsilon_{Hf}(t)$ values were calculated with reference to a chondritic uniform reservoir (CHUR). The $^{176}Lu/^{177}Hf$ and $^{176}Hf/^{177}Hf$ ratios used for the CHUR are 0.0336 and 0.282785, respectively (Bouvier et al., 2008). The single-stage model age (T_{DM1}) was calculated relative to the depleted mantle with present-day $^{176}Lu/^{177}Hf$ and $^{176}Hf/^{177}Hf$ ratios of 0.03933 and 0.283294, respectively (Blichert-Toft and Puchtel, 2010). The two-stage Hf model age (T_{DM2}), also interpreted as crust formation age, was calculated by projecting the zircon $^{176}Hf/^{177}Hf(t)$ back to the depleted-mantle model growth curve assuming a $^{176}Lu/^{177}Hf$ ratio of 0.01 for felsic crust and 0.02 for mafic crust.

4. Results

4.1. Petrography

The twelve gneissic granitoids in this study could be divided into three groups based on their mineral assemblages (Table 1): trondhjemites, biotite-granites, and two-mica granites. The trondhjemites contain the highest proportion of plagioclase (~50%) and the lowest of K-feldspar (5–10%), whereas the two-mica granites are the opposite, with only 5–20% plagioclase but 35–55% K-feldspar. The biotite-granites hold the moderate proportions of plagioclase (15–30%) and K-feldspar (25–40%). In addition, trondhjemites and biotite-granites only have biotite as the ferromagnesian mineral (Figs. 2a–c), whereas the two-mica granites contain both biotite (<5%) and muscovite (~1%) (Figs. 2d–f). The muscovite occurs as subhedral grains (Fig. 2e), inclusions in orthoclase (Fig. 2d), or relicts in biotite (Fig. 2f), indicating a primary origin. Accessory minerals like zircon, titanite, and magnetite are common (Table 1). Besides, ilmenite, apatite, chlorite, and goethite occur in a few samples as well (e.g., Fig. 2d).

4.2. Zircon CL images, U–Pb geochronology, and Lu–Hf isotope patterns

Zircon CL images are shown in Fig. 3. The U–Pb and Lu–Hf results are provided in Supplementary Table S3 and summarized in Table 2 and Figs. 4–6. In total, 278 U–Pb analyses were performed on 264 zircon grains, and 94 of them show age concordance between 98% and 102%. Furthermore, 170 Lu–Hf analyses were carried out on 164 grains. Initial $^{176}Hf/^{177}Hf$ ratios, referred to as $^{176}Hf/^{177}Hf(t)$, were calculated using the Lu–Hf isotopic data and the $^{207}Pb/^{206}Pb$ ages obtained from the same zircon domain. These ratios are almost identical to the initial $^{176}Hf/^{177}Hf$ calculated for the true zircon crystallization age (Supplementary Table S3), due to the low Lu/Hf in zircon (Gerdes and Zeh, 2009).

We use the combined CL images and the U–Pb and Lu–Hf data to discriminate different zircon growth and/or alteration events (Zeh et al., 2007, 2009; Gerdes and Zeh, 2009). As shown in CL images (Fig. 3), many grains show typical oscillatory or linear magmatic zoning patterns. However, some grains reveal complex core-rim structures (e.g., Figs. 3-1, -4, -5, and -23). The rims show features typical of alteration/reaction fronts (e.g., Geisler et al., 2007), following or transecting former zircon zoning patterns. A few grains contain inherited zircon cores with apparently older ages than other zircon domains (Figs. 3-12 and -18). For most samples, the combined U–Pb and Lu–Hf datasets reveal simple patterns when plotted in $^{176}Hf/^{177}Hf(t)$ vs. $^{207}Pb/^{206}Pb$ age diagrams (Fig. 5). In general, two groups can be distinguished.

(1) *Group I*. Samples in this group reveal only one zircon generation for each sample (Table 2), include trondhjemites KH254 (Figs. 4a and 5a) and KH256 (Figs. 4b and 5b) as well as two-mica granites KH196 (Figs. 4g and 5g) and KH231 (Figs. 4l and 5l). These zircons show typical magmatic oscillatory zoning (Fig. 3) and high Th/U ratios (mostly among 0.2–1.0; down to 0.05 for a few altered grains) (Supplementary Table S3), indicative of a magmatic origin. All analyzed zircon domains in each sample show large variations in $^{207}Pb/^{206}Pb$ ages (positively correlated to age concordance) but yield within error identical $^{176}Hf/^{177}Hf(t)$, resulting in a horizontal array in the $^{176}Hf/^{177}Hf(t)$ vs. $^{207}Pb/^{206}Pb$ age diagram (Figs. 5a, b, g, and l). This indicates that all zircons within each sample formed at the same time (most probably during magma crystallization), but suffered variable Pb loss due to later alteration. This alteration caused resetting of the U–Pb system but left the Hf isotope system intact (e.g., Amelin et al., 2000; Gerdes and Zeh, 2009; Guo et al., 2014b). The concordant and discordant zircons together yield well-defined upper intercept ages in the concordia diagrams, which we interpret as the time of magma intrusion (Fig. 4; Table 2).

(2) *Group II*. This group comprises all the rest samples, including KH258 (Figs. 4c and 5c), KH201 (Figs. 4d and 5d), KH244 (Figs. 4e and 5e), KH229 (Figs. 4f and 5f), KH233 (Figs. 4h and 5h), KH216 (Figs. 4i and 5i), KH199 (Figs. 4j and 5j), and KH234 (Figs. 4l and 5l). Most of them reveal two zircon populations (Table 2). One population shows features similar to those in Group I, for instance, (1) typical magmatic oscillatory or linear zoning patterns (Fig. 3), (2) Th/U ratios >0.2 (with a few exceptions) (Supplementary Table S3), (3) within error identical $^{176}Hf/^{177}Hf(t)$ against scattered $^{207}Pb/^{206}Pb$ ages (e.g., Figs. 5c, d, and k). As discussed above, such features suggest these zircons in each sample were crystallized from the same magma at the same time, but experienced one or multiple Pb loss via alteration. We interpret the upper intercept ages of the magmatic zircons as the emplacement ages of magmas (Fig. 4; Table 2).

The major difference between Group I and II is that the samples in Group II contain a younger zircon population (possibly formed at ca. 2.0 Ga). These zircons show low luminance and lack of internal zoning in the CL images (e.g., Figs. 3-7 and -23). Their Th/U ratios are generally low (down to 0.01) (Supplementary Table S3), suggestive of a metamorphic origin. They are commonly discordant,

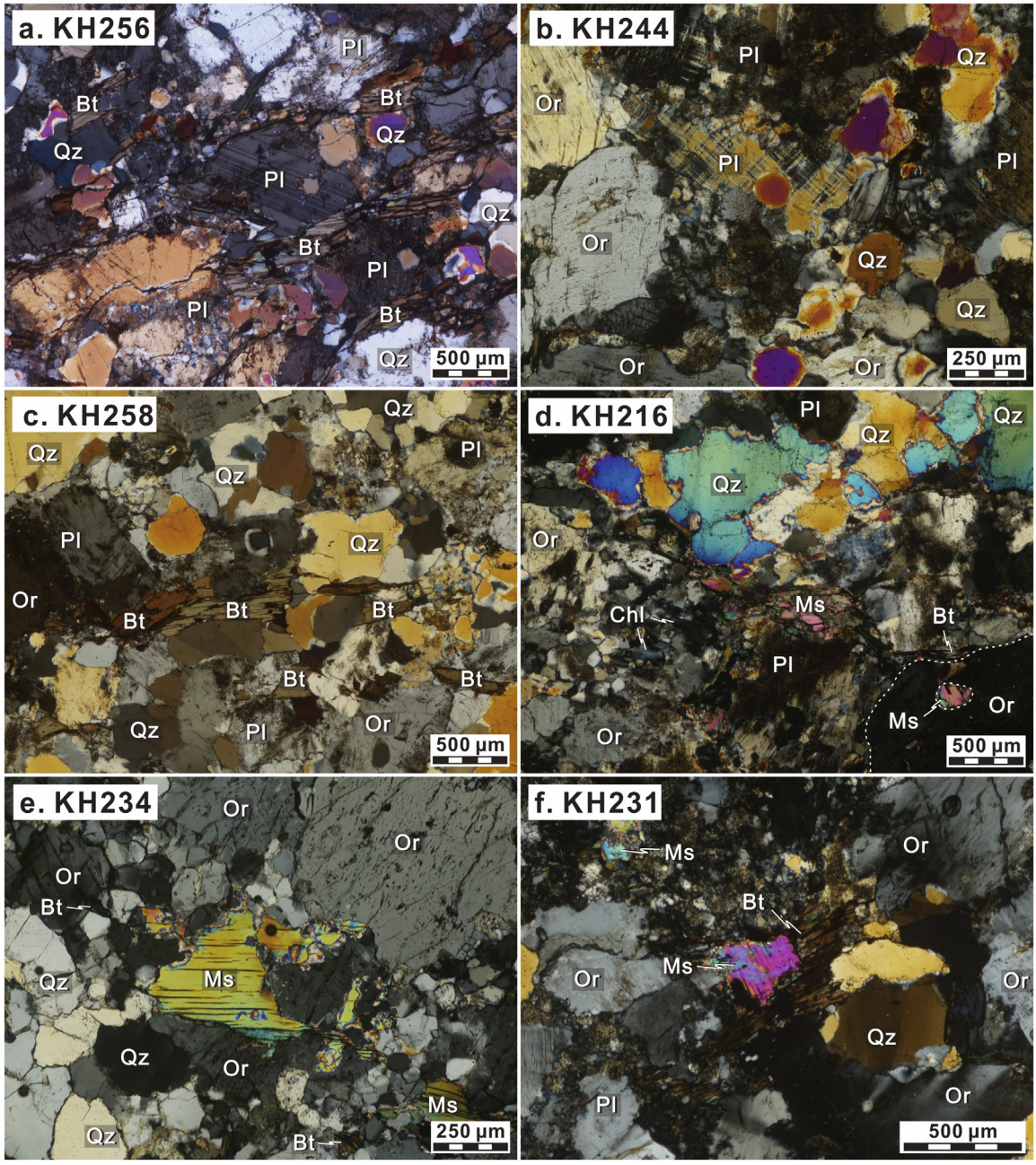

Fig. 2. Optical micrographs under cross-polarized lights for gneissic granitoids from the Kongling Terrane. (a) 3.29 Ga trondhjemite KH256. (b) 2.79 Ga biotite granite KH244. (c) 2.81 Ga biotite granite KH258. (d) 2.64 Ga two-mica granite KH216, where one muscovite inclusion is present in orthoclase. The dashed line indicates the grain boundary of orthoclase. (e) 2.42 Ga two-mica granite KH234. (f) 2.00 Ga two-mica granite KH231, in which muscovite is overgrown by biotite. Mineral abbreviations (Whitney and Evans, 2010): Qz, quartz; Pl, plagioclase; Or, orthoclase; Bt, biotite; Ms, muscovite; Chl, chlorite; Zrn, zircon.

defining another discordia line in the U–Pb concordia diagrams, in addition to the discordia line defined by older magmatic zircons with Archean ages (e.g., Figs. 4c, d, f, i, j, and k). Thus, it can be seen in the concordia diagrams that the magmatic zircons together with the metamorphic zircons actually spread within a "fan" limited by an upper intercept with Archean ages and two lower intercepts at roughly 2 Ga and <0.5 Ga. This indicates a mixed effect of ancient and recent Pb loss. Most metamorphic zircons show comparable $^{176}Hf/^{177}Hf(t)$ to the older magmatic zircons, suggesting their formation by recrystallization, whereas a few grains show much higher $^{176}Hf/^{177}Hf(t)$, indicating new metamorphic growth (e.g., Figs. 5c, d, f, i, j, and k) (Gerdes and Zeh, 2009; Chen et al., 2010). Another difference between Group I and II is that several Group-II samples (e.g., KH258, KH233, and KH199) contain minor inherited zircon cores. Such inherited zircons can be distinguished by CL images (e.g., Figs. 3-15, -18, and -19), apparently older ages (3.4–2.8 Ga) (Figs. 4c, f, h, and j), and low $^{176}Hf/^{177}Hf(t)$ (Figs. 5c, h, and j). Their distinct $^{176}Hf/^{177}Hf(t)$ from younger magmatic and metamorphic zircons indicate that they were formed by different magmatic/metamorphic events.

In summary, the two trondhjemites KH254 and KH256 show identical emplacement ages 3313 ± 30 Ma (n = 20) and 3292 ± 33 Ma (n = 17), respectively. The five biotite-granites yield intrusion ages of 2810 ± 49 Ma (n = 14) for KH258, 2803 ± 27 Ma (n = 19) for KH201, 2785 ± 43 Ma (n = 4) for KH244, 2781 ± 26 Ma (n = 11) for KH229, and 2662 ± 20 Ma (n = 33) for KH233. The five two-mica granites show scattered emplacements ages. Three

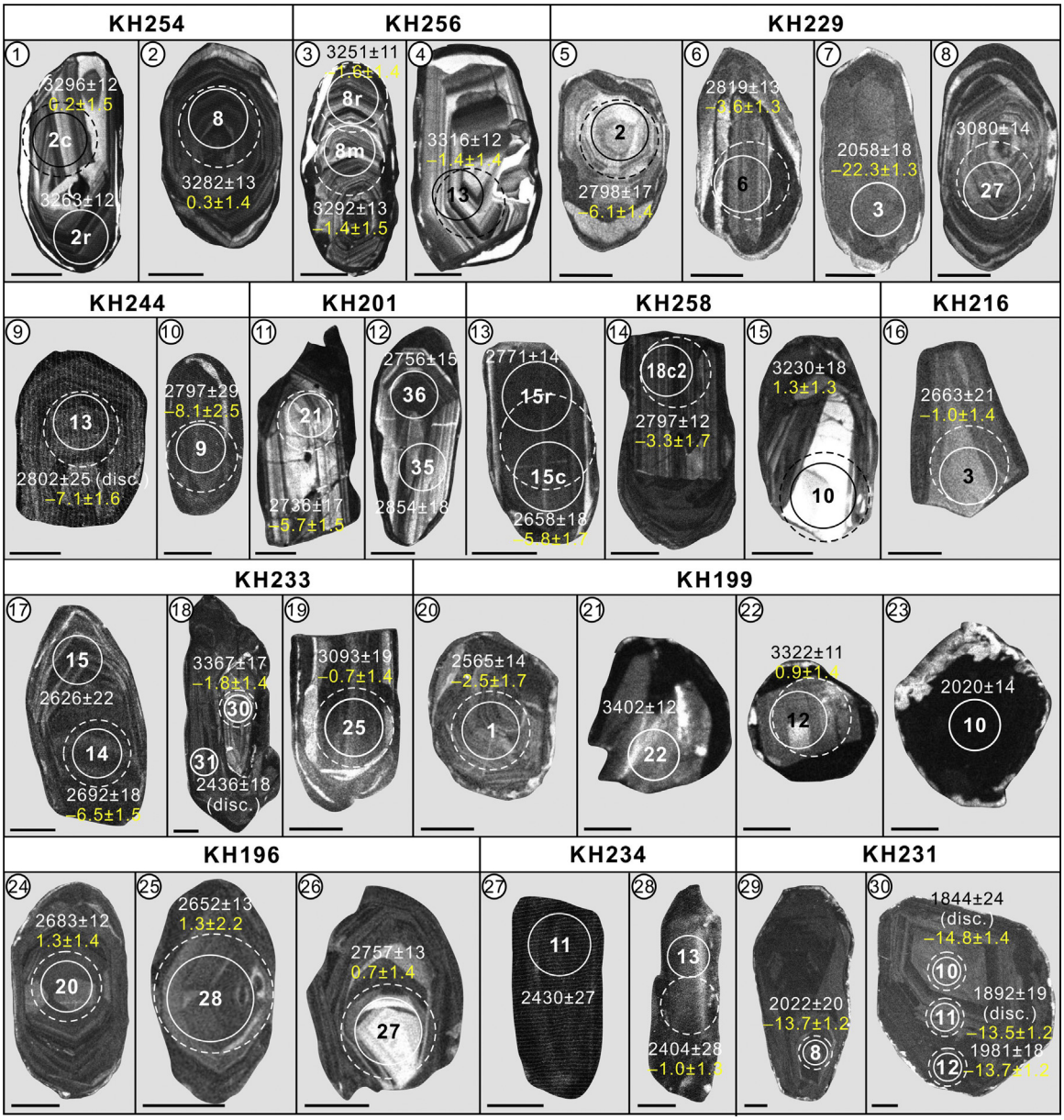

Fig. 3. Cathodoluminescence images of concordant zircons with age concordance between 98% and 102%. The solid and dashed circles represent spots for LA-ICP-MS U–Pb and LA-MC-ICP-MS Lu–Hf isotope analyses, respectively. Grain numbers are shown in the center of the circles, while their $^{207}Pb/^{206}Pb$ ages (in Ma) and $\varepsilon_{Hf}(t)$ values with 1σ uncertainties are listed next to the circles. The white bars correspond to a length of 30 μm. *Abbreviation*: disc., discordant.

of them (KH196, KH216, and KH199) yield emplacement ages of 2695 ± 23 Ma (n = 30), 2638 ± 26 Ma (n = 2), and 2636 ± 51 Ma (n = 18), respectively. The rest two samples KH234 and KH231 show intrusion ages of 2418 ± 52 Ma (n = 5) and 2004 ± 19 Ma (n = 16), respectively. The ages and Hf isotopic compositions of the magmatic, metamorphic, and inherited zircons in each sample are summarized in Table 2 and shown in Figs. 4–6.

4.3. Whole-rock major and trace element compositions

The major and trace element compositions of the gneissic granitoid are listed in Table 3. According to normative feldspar compositions, these samples are recognized as two trondhjemites and ten granites (Fig. 7a). All samples have 70.61–74.61 wt% SiO_2 and 13.83–15.36 wt% Al_2O_3 (Fig. 8). They are magnesian and weakly peraluminous (A/CNK 1.04–1.15) (Figs. 7b and c). The two trondhjemites are rich in Na_2O (4.67–4.70 wt%) but poor in K_2O (1.98–2.38 wt%); they also show high $Mg^{\#}$ (45–47), MgO (1.15–1.19 wt%), TFe_2O_3 (2.67–2.73 wt%), and CaO (2.00–2.13 wt%) contents (Fig. 8). Their trace elements are characterized by enriched large ion lithophile elements (LILEs), depleted high field strength elements (HFSEs) (e.g., Ti, Nb, Ta, and P), low Cr (0.54–3.08 ppm) and Ni (2.14–5.56 ppm) concentrations. They show moderate amounts of heavy rare earth elements (HREEs) (e.g., 0.79–1.70 ppm Yb), relatively low Sr/Y (12–33) and La_N/Yb_N (8–16), and depleted Eu (Eu/Eu^* 0.63–0.91) (Figs. 9a and b; Table 3). These characteristics make them similar to the medium-pressure TTGs described by Moyen and Martin (2012) (Figs. 9a and b).

The ten granites show different chemical features from the 3.3 Ga trondhjemites (Fig. 8). They are characterized by higher K_2O contents (3.29–6.71 wt%) and lower $Mg^{\#}$ (30–45, with one exception of 55), MgO (0.18–0.59 wt%), TFe_2O_3 (0.63–1.89 wt%), and CaO (0.43–1.23 wt%) contents (Fig. 8). They show (1) more pronounced enrichment of LILEs and depletion of HFSEs, (2) low total

Table 2
Summary of U–Pb ages and Lu–Hf isotopic compositions of different zircon types in gneissic granitoids from the Kongling Terrane.

Sample	Group	Rock type	Zircon type		U–Pb ages			Hf isotopic compositions			
					Age (Ma)	*N*	Type	$^{176}Hf/^{177}Hf(t)$	$\varepsilon_{Hf}(t)$	T_{DM2} (Ga)	*N*
KH254	I	Trondhjemite	I	Magmatic	3313 ± 30	20	Upper intercept age	0.280638 ± 13	0 ± 0.5	3.70 ± 0.03	11
KH256	I	Trondhjemite	I	Magmatic	3292 ± 33	17	Upper intercept age	0.280629 ± 10	−0.8 ± 0.4	3.75 ± 0.03	18
KH258	II	Biotite-granite	I	Magmatic	2810 ± 49	14	Upper intercept age	0.280833 ± 19	−4.9 ± 0.7	3.41 ± 0.03	13
			II	Metamorphic	2003 ± 18	5	Upper intercept age	0.280915 ± 45			3
								0.281209			1
			III	Inherited	3230 ± 18	1	$^{207}Pb/^{206}Pb$ age	0.280733	1.3	3.43	1
KH201	II	Biotite-granite	I	Magmatic	2803 ± 27	19	Upper intercept age	0.280872 ± 20	−3.8 ± 0.7	3.35 ± 0.04	10
			II	Metamorphic	2021 ± 59	7	Upper intercept age				
KH244	II	Biotite-granite	I	Magmatic	2785 ± 43	4	Upper intercept age	0.280775 ± 15	−7.7 ± 0.5	3.53 ± 0.04	4
			II	Metamorphic	2040–1860 (disc.)	2	$^{207}Pb/^{206}Pb$ age	0.280872 ± 31			2
KH229	II	Biotite-granite	I	Magmatic	2781 ± 26	11	Upper intercept age	0.280801 ± 11	−6.9 ± 0.4	3.47 ± 0.02	6
			II	Metamorphic	2026 ± 21	8	Upper intercept age	0.280913 ± 27			6
			III	Inherited	3080 ± 14	14	$^{207}Pb/^{206}Pb$ age				
					2888 ± 18	18	$^{207}Pb/^{206}Pb$ age	0.280781	−5.1	3.47	1
KH196	I	Two-mica granite	I	Magmatic	2695 ± 23	30	Upper intercept age	0.281077 ± 16	1.0 ± 0.6	3.03 ± 0.03	16
KH233	II	Biotite-granite	I	Magmatic	2662 ± 20	33	Upper intercept age	0.280936 ± 19	−4.9 ± 0.7	3.29 ± 0.03	19
			II	Metamorphic	1951 ± 35 (disc.)	1	$^{207}Pb/^{206}Pb$ age				
			III	Inherited	3367 ± 17	1	$^{207}Pb/^{206}Pb$ age	0.280553	−1.8	3.7	1
					3093 ± 19	1	$^{207}Pb/^{206}Pb$ age	0.280767	−0.7	3.43	1
KH216	II	Two-mica granite	I	Magmatic	2638 ± 26	2	Weighted mean	0.281066 ± 9	−0.8 ± 0.3	3.07 ± 0.02	2
			II	Metamorphic	2004 ± 33	9	Upper intercept age	0.281027			1
								0.281190 ± 21			3
KH199	II	Two-mica granite	I	Magmatic	2636 ± 51	18	Upper intercept age	0.280997 ± 21	−3.2 ± 0.8	3.19 ± 0.04	13
			II	Metamorphic	2031 ± 50	4	Upper intercept age	0.281062			1
			III	Inherited	3402 ± 12	1	$^{207}Pb/^{206}Pb$ age				
					3322 ± 11	1	$^{207}Pb/^{206}Pb$ age	0.280661	0.9	3.53	1
					3278 ± 13	1	$^{207}Pb/^{206}Pb$ age				
					3274 ± 14	1	$^{207}Pb/^{206}Pb$ age	0.280625	−1.5	3.61	1
					3227 ± 11	1	$^{207}Pb/^{206}Pb$ age	0.280640	−2.1	3.59	1
KH234	II	Two-mica granite	I	Magmatic	2418 ± 52	5	Upper intercept age	0.280919 ± 24	−11.2 ± 0.9	3.42 ± 0.04	5
			II	Metamorphic	1924 ± 61	2	Upper intercept age	0.280921			1
			III	Inherited	2568 ± 42 (disc.)	1	$^{207}Pb/^{206}Pb$ age	0.280897	−8.5	3.39	1
KH231	I	Two-mica granite	I	Magmatic	2004 ± 19	16	Upper intercept age	0.281143 ± 10	−12.8 ± 0.4	3.15 ± 0.02	16

Uncertainties for $^{207}Pb/^{206}Pb$ ages are 1σ, while those for intercept ages, $^{176}Hf/^{177}Hf(t)$, $\varepsilon_{Hf}(t)$, and two-stage model ages (T_{DM2}) are all 2σ.

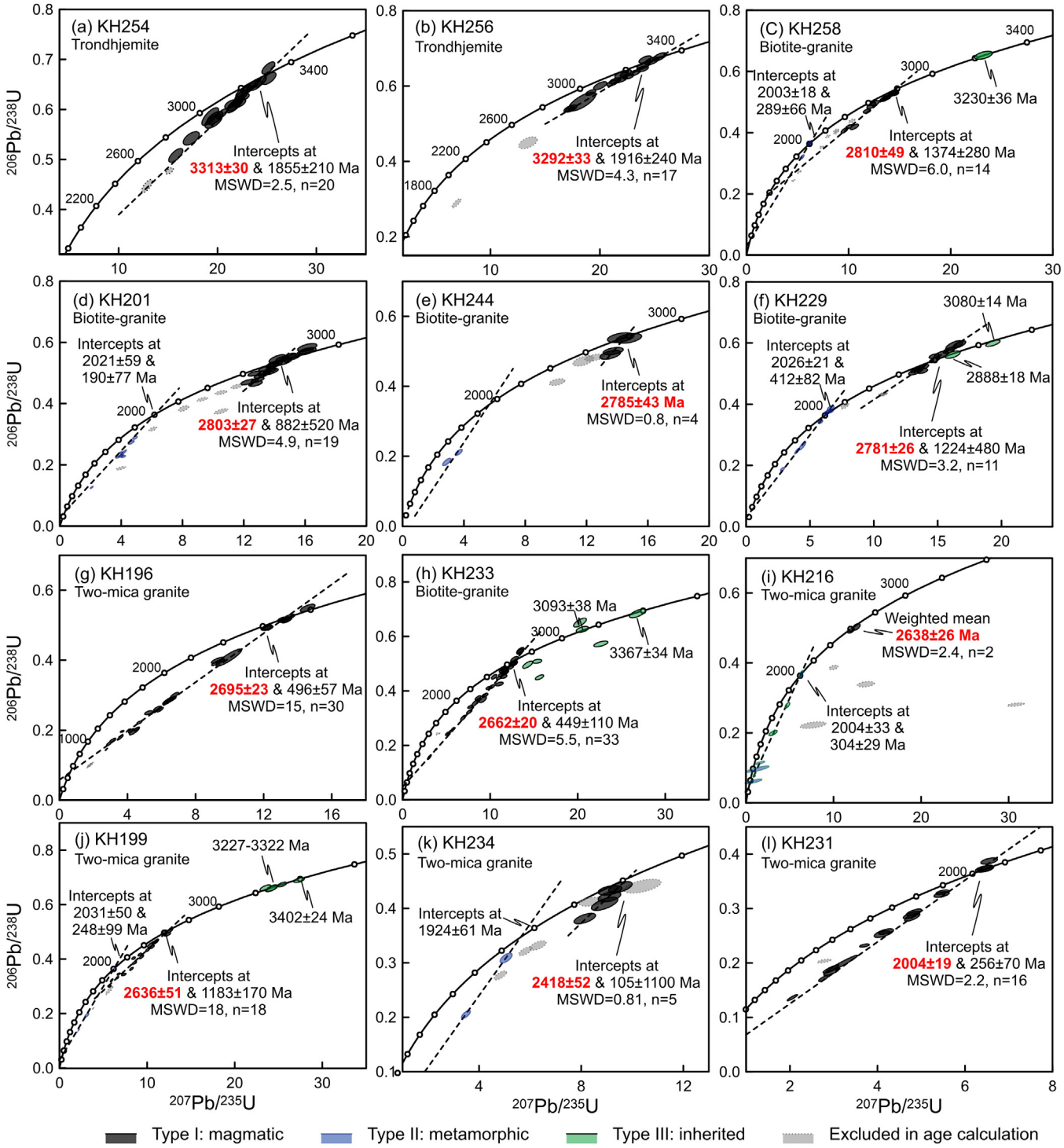

Fig. 4. Zircon U–Pb concordia diagrams for gneissic granitoids from the Kongling Terrane. Data-point error ellipses are 2σ. The grey dashed ellipses indicate the analyses that were excluded from age calculations. Uncertainties of the intercept ages and weighted mean ages are given at 2σ level.

REEs (45–96 ppm, with one exception of 171 ppm), (3) variable Eu anomalies (Eu/Eu* 0.51–5.39), and (4) scattered La_N/Yb_N (11–46) and Sr/Y (10–95) (Figs. 9g–n). Their transitional metal element contents are low (e.g., 0.54–3.08 ppm Cr and 2.14–5.56 ppm Ni). The 2.8 Ga biotite-granites also show higher Zr–Hf contents relative to other elements (Fig. 9g). Specifically, the 2.0 Ga two-mica granite KH231 exhibits a different trace element pattern, characterized by strong positive Ba, Sr, and Eu anomalies (e.g., Eu/Eu* 4.73–5.54) and the lowest REE content (63–65 ppm) (Figs. 9m and n).

5. Discussion

5.1. Petrogenesis of the episodic granitoid magmatism in the Kongling Terrane

Together with previously reported Archean-Paleoproterozoic igneous rocks (Zhang et al., 2006a; Zheng et al., 2006; Jiao et al., 2009; Peng et al., 2009, 2012; Xiong et al., 2009; Gao et al., 2011; Wei and Wang, 2012; Chen et al., 2013; Guo et al., 2014b; Li

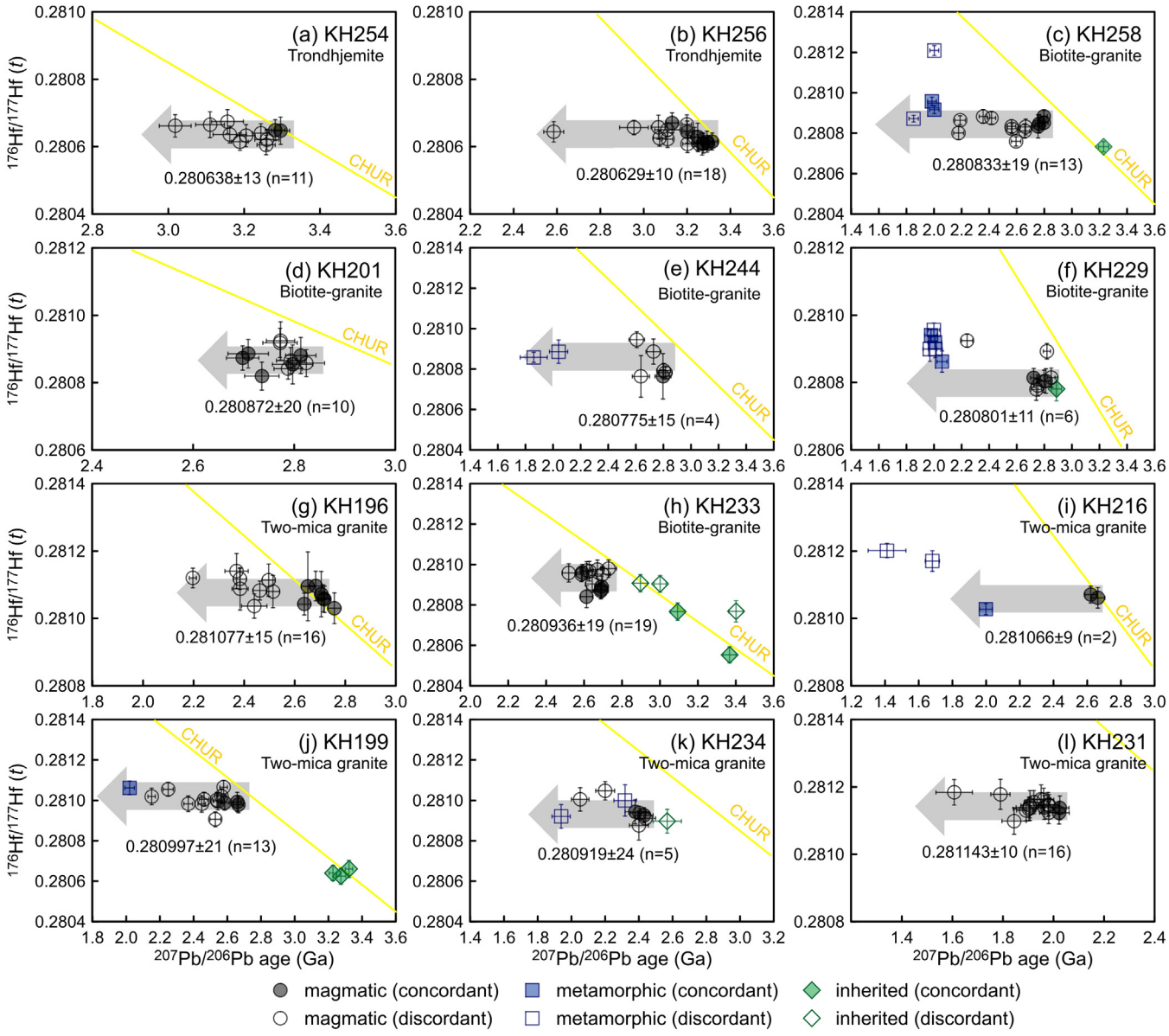

Fig. 5. Plots of $^{207}Pb/^{206}Pb$ age vs. $^{176}Hf/^{177}Hf(t)$ for gneissic granitoids from the Kongling Terrane. The circles, squares, and diamonds indicate magmatic, metamorphic, and inherited zircons, respectively. The filled symbols denote concordant analyses with age concordance between 98% and 102%, while the open symbols represent discordant analyses. Error bars are $\pm 2\sigma$. The numbers indicate mean $^{176}Hf/^{177}Hf(t)$ with 2σ errors calculated from both the concordant and the discordant magmatic zircons. The grey arrows indicate the recrystallization-induced Pb loss trend. The solid lines indicate the evolution trend of a chondritic uniform reservoir (Bouvier et al., 2008).

et al., 2014), two major (3.0–2.9 and 2.7–2.6 Ga) and five minor (3.45, 3.3–3.2, 2.8, 2.4, and 2.0–1.85 Ga) granitoid episodes could be revealed in the Kongling Terrane (Fig. 10). The nature of the granitoid sources, crustal evolution (reworking or growth), and geodynamic implications are discussed as followings. The uncertainties for ages and mean values in the discussion are given at 2σ level, if not specifically indicated.

5.1.1. Early TTG-dominated magmatic stage

5.1.1.1. 3.3 and 3.2 Ga TTG magmatism. The emplacement ages (3.31 and 3.29 Ga) of the two trondhjemites (KH254 and KH256) in this study confirm the existence of 3.3 Ga TTG magmatism in the Yangtze Craton (Gao et al., 2011). Their major element compositions are similar to the partial melts from low-K metabasalts as determined by experimental studies (Fig. 11). On one hand, these samples show low Sr (264–326 ppm) and Ba (284–541 ppm) contents as well as negative Eu anomalies (Eu/Eu^{*} 0.63–0.91) (Table 3), indicating that plagioclase may have existed as a residual or fractionated phase. On the other hand, the moderate amounts of HREEs (e.g., 0.79–1.70 ppm Yb) and relatively high La_N/Yb_N (8–16) and Sr/Y ratios (12–33) (Figs. 9a and b; Table 3) are similar to those of the typical medium-pressure TTGs, supporting the presence of garnet in the source region (Moyen, 2011; Moyen and Martin, 2012). The coexistence of garnet and plagioclase indicate a garnet amphibolite-facies source with pressures over 10 kbar (>30 km deep) (Moyen, 2011). The chondritic $\varepsilon_{Hf}(t)$ values (−0.8 to 0) and Eoarchean T_{DM2} (3.75–3.70 Ga) suggest that this source crust might be long lived (>0.4 Ga), if it were derived from a depleted mantle source (Fig. 6b). Alternatively, this mafic crustal could be generated from a near-primordial mantle source (i.e., fertile lower mantle), which may possess a chondritic Lu–Hf isotopic composition (Guitreau et al., 2012; Martin et al., 2014). There are two common tectonic scenarios to produce TTG magmatism: (1) melting of subducted oceanic crust and (2) melting at the base of a mafic crust (e.g., Drummond and Defant, 1990; Smithies, 2000; Martin and Moyen, 2002; Condie, 2005b; Martin et al., 2005, 2014; Hoffmann et al.,

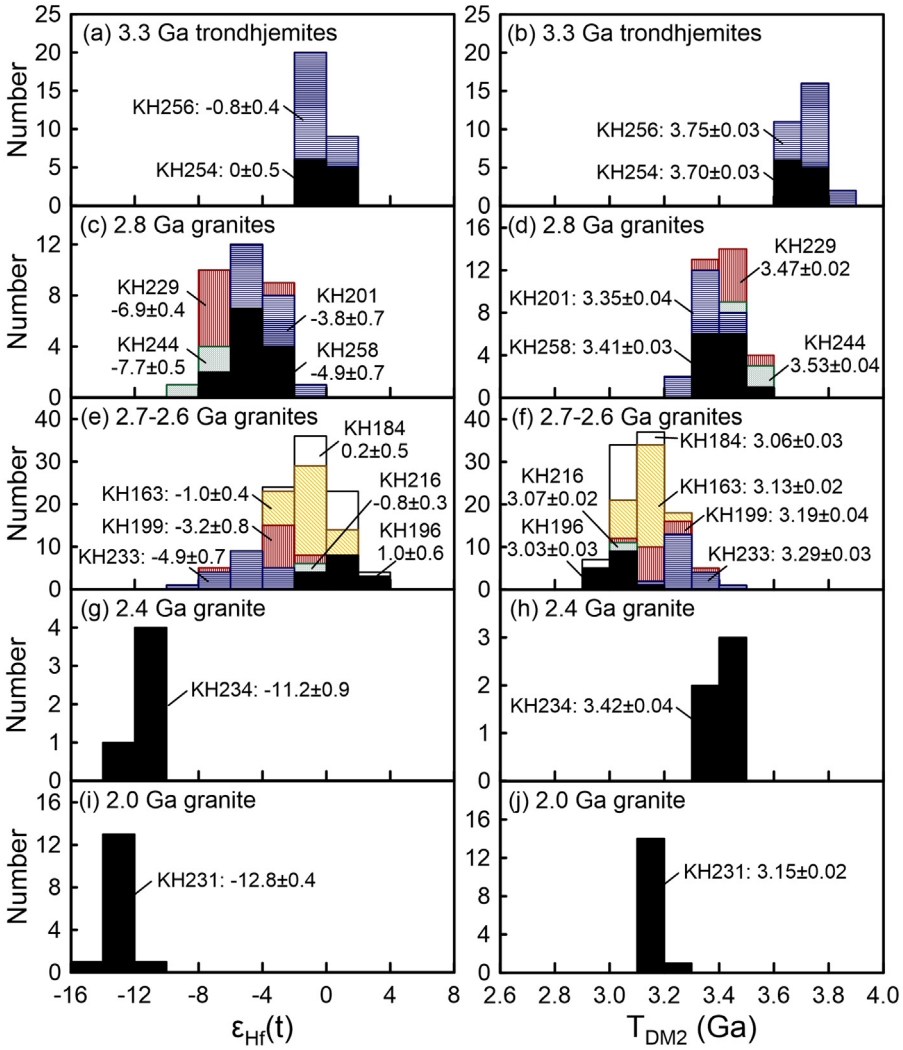

Fig. 6. Histograms of $\varepsilon_{Hf}(t)$ values (left panel) and two-stage Hf model ages (T_{DM2}) (right panel) for magmatic zircons in gneissic granitoids from the Kongling Terrane.

2011; Moyen, 2011; Moyen and Martin, 2012). Subduction-related TTG magmas tend to possess higher Mg#, Cr and Ni contents as well as suprachondritic $\varepsilon_{Hf}(t)$ values, due to interactions between the TTG melts and the mantle wedge (e.g., Smithies, 2000; Martin and Moyen, 2002; Martin et al., 2005; Moyen and Martin, 2012). However, the 3.3 Ga trondhjemites have low Cr (19.0–19.8 ppm) and Ni (18.4–18.6 ppm) contents and only chondritic $\varepsilon_{Hf}(t)$ values, indicating limited, if not absent, interactions of the trondhjemitic melt with the mantle (Tables 3; Fig. 6a). Therefore, it is more likely that the 3.3 Ga trondhjemites were derived at the base of a thick mafic crust, e.g., an oceanic plateau.

3.2 Ga orthogneisses, mostly trondhjemites (Y.B. Wu's unpublished data), have been reported from the northern margin of the North Kongling Terrane (Jiao et al., 2009). Given that 3.2 Ga inherited zircons are common in younger TTG and granitic rocks (Qiu et al., 2000; Zhang et al., 2006a; Chen et al., 2013), 3.2 Ga rocks may be more widespread than presently exposed. The 3.2 Ga orthogneisses display subchondritic mean $\varepsilon_{Hf}(t)$ values (-2.33 ± 0.51), suggesting reworking of a long-existed mafic crust. They also exhibit (1) comparable major element compositions (suggesting mafic source rocks as well; Figs. 8 and 11), (2) identical Eoarchean T_{DM2} (mean 3.68 ± 0.05 Ga) (Jiao et al., 2009), and (3) similarly low Cr (7.3–17.0 ppm) and Ni (6.0–15.8 ppm) concentrations (Fig. 12) to those of the 3.3 Ga trondhjemites. These features suggest that the 3.2 Ga TTGs may have formed by a similar mechanism as for the 3.3 Ga ones, that is, melting at the base of a pre-existing mafic crust with few contributions from the mantle. However, the 3.2 Ga orthogneisses have more depleted HREEs (e.g., 0.22–0.74 ppm Yb) and HFSEs as well as increased La_N/Yb_N (54–235) and Sr/Y (53–152) ratios (Figs. 9c, d, and 12; Table 3), which indicates the presence of more abundant garnet and less plagioclase in the source region, possibly in eclogite facies with a higher pressure >15 kbar (at depth >50 km) (Moyen, 2011). Thus, the 3.2 Ga TTGs may have been derived from the base of an over-thickened mafic crust, further implying a crustal thickening event in the Kongling Terrane during 3.3–3.2 Ga.

5.1.1.2. 3.0–2.9 Ga TTG magmatism. The 3.0–2.9 Ga TTG rocks are widespread in the North Kongling Terrane (Qiu et al., 2000; Zhang et al., 2006a; Zheng et al., 2006; Gao et al., 2011; Chen et al., 2013; Li et al., 2014). Their major element compositions mostly fall into the field of partial melts from low-K mafic rocks (Fig. 11). They show weak Eu and Sr anomalies, low HREEs (e.g., 0.32–1.12 ppm Yb), as well as high La_N/Yb_N (23–107) and Sr/Y (23–196) ratios, indicating an eclogite-facies source region (Moyen, 2011) (Figs. 9e, f, and 12h). The 3.0–2.9 Ga TTGs also exhibit variable Mg# (34–59), Cr (3.39–106 ppm), and Ni (4.14–75.3 ppm) contents (Gao et al., 1999, 2011; Chen et al., 2013), which could be explained by interactions of the TTG melts with mantle rocks, possibly in a subduction zone (e.g., Smithies, 2000; Martin and Moyen, 2002;

Table 3
Chemical compositions of gneissic granitoids from the Kongling Terrane.

Sample	KH254	KH256	KH201	KH229	KH229R	KH244	KH196	KH233	KH199	KH216	KH234	KH234R	KH231
Major element contents (wt%)													
SiO_2	71.39	70.61	72.46	73.29	73.13	74.32	73.68	74.61	73.65	74.46	72.62	72.51	71.47
TiO_2	0.30	0.32	0.10	0.14	0.13	0.08	0.09	0.07	0.07	0.13	0.25	0.24	0.16
Al_2O_3	14.28	14.99	15.36	14.59	14.57	14.42	14.83	14.32	14.25	13.83	14.62	14.62	15.25
TFe_2O_3	2.73	2.67	0.86	1.18	1.17	0.63	0.84	0.82	0.81	0.89	1.88	1.89	1.24
MnO	0.03	0.04	0.01	0.01	0.01	0.01	0.01	0.01	0.01	0.01	0.02	0.02	0.01
MgO	1.15	1.19	0.30	0.43	0.41	0.26	0.25	0.18	0.50	0.30	0.58	0.59	0.43
CaO	2.13	2.00	1.20	1.23	1.22	1.10	0.66	0.91	0.43	1.17	0.94	0.94	1.00
Na_2O	4.67	4.70	4.22	4.32	4.29	4.25	5.55	4.03	2.87	3.75	3.99	3.95	3.23
K_2O	1.98	2.38	4.51	4.07	4.06	4.04	3.29	4.54	6.71	4.52	4.13	4.14	6.17
P_2O_5	0.18	0.10	0.03	0.03	0.03	0.02	0.05	0.03	0.03	0.04	0.08	0.08	0.05
LOI	0.82	0.80	0.63	0.48	0.49	0.46	0.45	0.32	0.60	0.59	0.99	0.97	0.54
Total	99.66	99.80	99.68	99.77	99.51	99.59	99.70	99.84	99.93	99.69	100.10	99.95	99.55
$Mg^{\#}$	45	47	41	42	41	45	37	30	55	40	38	38	41
A/NK	1.45	1.45	1.30	1.27	1.27	1.27	1.17	1.24	1.19	1.25	1.33	1.33	1.27
A/CNK	1.04	1.08	1.10	1.06	1.07	1.08	1.07	1.09	1.12	1.05	1.15	1.15	1.10
Trace element concentrations (ppm)													
Sc	5.68	3.91	1.56	1.41	1.44	1.36	1.21	2.01	1.81	1.45	2.86	2.86	1.14
V	30.6	27.4	6.86	10.08	8.91	4.91	6.23	3.34	5.54	7.90	13.2	12.0	14.5
Cr	19.8	19.0	0.75	0.58	0.64	0.99	1.85	0.58	2.29	3.08	2.54	2.30	1.04
Ni	18.6	18.4	3.26	3.86	3.94	3.06	2.51	2.14	5.56	4.57	3.82	3.88	3.65
Rb	93.3	78.0	97.9	79.9	78.4	64.0	78.4	104	101	155	131	132	125
Sr	264	326	327	311	306	291	369	159	202	149	235	234	611
Y	21.4	9.76	6.82	3.27	3.24	6.81	6.54	15.9	9.45	6.67	12.4	12.5	2.50
Zr	127	114	81.4	144	131	60.0	83.0	97	77.9	84.4	171	178	338
Nb	16.0	7.65	3.06	5.57	5.55	2.22	4.56	2.44	5.12	4.51	8.31	8.17	2.23
Ba	284	541	986	1294	1264	859	1160	511	1168	658	1143	1169	2983
La	19.1	18.7	16.6	15.7	15.9	10.9	17.6	21.8	22.3	19.4	40.1	40.0	19.5
Ce	41.6	33.6	30.0	28.8	29.1	18.9	37.6	40.8	44.5	35.7	80.3	80.2	29.2
Pr	4.17	3.89	3.01	2.99	3.05	1.99	3.40	4.21	4.38	3.66	8.02	8.11	2.69
Nd	15.2	14.3	10.55	10.5	10.4	6.93	11.8	14.6	15.4	12.6	27.6	27.7	9.00
Sm	3.39	2.72	1.80	1.61	1.68	1.31	2.23	3.09	2.73	2.24	4.91	4.88	1.02
Eu	0.69	0.71	0.65	0.54	0.53	0.46	0.57	0.47	0.71	0.62	0.99	1.00	1.41
Gd	3.26	2.09	1.46	1.01	1.12	1.16	1.55	2.59	2.11	1.62	3.25	3.25	0.62
Tb	0.53	0.33	0.20	0.12	0.12	0.17	0.22	0.39	0.32	0.22	0.44	0.46	0.075
Dy	3.18	1.80	1.11	0.50	0.54	1.04	1.20	2.41	1.59	1.21	2.37	2.42	0.38
Ho	0.62	0.33	0.21	0.094	0.093	0.21	0.21	0.50	0.32	0.21	0.44	0.43	0.079
Er	1.78	0.91	0.61	0.28	0.27	0.71	0.56	1.53	0.88	0.55	1.17	1.10	0.24
Tm	0.28	0.14	0.092	0.044	0.046	0.11	0.083	0.24	0.14	0.074	0.16	0.16	0.034
Yb	1.70	0.79	0.60	0.33	0.29	0.69	0.55	1.40	0.91	0.49	1.01	0.93	0.29
Lu	0.26	0.12	0.085	0.056	0.049	0.11	0.078	0.20	0.13	0.071	0.15	0.15	0.046
Hf	3.54	3.18	2.59	4.27	4.04	2.03	2.97	3.65	2.76	2.47	4.90	5.07	7.99
Ta	2.11	0.90	0.30	0.44	0.45	0.27	0.44	0.29	0.43	0.48	0.57	0.57	0.48
Pb	122	13.0	28.8	22.8	22.4	33.0	21.2	29.6	41.6	28.6	38.9	39.1	23.1
Th	6.94	5.26	6.57	5.88	5.82	3.99	8.62	11.2	13.1	10.3	16.4	16.6	7.55
U	1.25	0.84	0.58	0.72	0.70	0.60	0.85	2.75	1.66	1.56	2.05	2.05	1.15
ΣREE	96	80	67	63	63	45	78	94	96	79	171	171	65
Eu/Eu^*	0.63	0.91	1.22	1.29	1.19	1.12	0.94	0.51	0.91	0.99	0.76	0.76	5.39
La_N/Yb_N	8	16	19	33	37	11	22	11	17	27	27	29	46
Sr/Y	12	33	48	95	94	43	56	10	21	22	19	19	244

R, reduplicate; $Mg^{\#}$, atomic $Mg/(Mg+Fe_{total})\times 100$; A/NK, molar $Al_2O_3/(Na_2O+K_2O)$; A/CNK, molar $Al_2O_3/(CaO+Na_2O+K_2O)$; Eu/Eu^*, $2\times Eu_N/(Sm_N+Gd_N)$. Normalization uses chondrite values from McDonough and Sun (1995).

Martin et al., 2005; Moyen and Martin, 2012). Mafic lenses or veins hosted in the 3.0–2.9 Ga TTGs (Wei and Wang, 2012; Wei and Jing, 2013; Li et al., 2014) display chemical affinities to typical island arc basalts, lending support to the subduction regime (Li et al., 2014). The possible tectonic settings include an oceanic island arc setting (Li et al., 2014) and a continental arc setting. In oceanic island arcs, however, both the subducting and the overriding plates are juvenile oceanic crusts. Thus, granitoids produced in such environments would exhibit radiogenic Hf isotopic compositions, with depleted mantle-like $\varepsilon_{Hf}(t)$ values (e.g., Schaltegger et al., 2002). This is in conflict to the unradiogenic nature in the 3.0–2.9 Ga TTG zircons, which exhibit a wide range of $\varepsilon_{Hf}(t)$ with predominant subchondritic values (Fig. 13). The >3.2 Ga T_{DM2} and minor 3.2 Ga inherited zircons in the 3.0–2.9 Ga TTGs (Zhang et al., 2006a) indicate a vital role of the ancient crystalline basement in the their genesis, which actually fits a continental arc setting. In continental arcs, due to melting and/or contamination of the overriding thick ancient continental crust above the subduction zone, granitoid magmas therein are commonly imprinted by less radiogenic Hf features characterized by lower $\varepsilon_{Hf}(t)$ values (e.g., Li et al., 2012; Ducea et al., 2015; Jones et al., 2015). Therefore, it is suggested that the tectonic environment of the Kongling Terrane during 3.0–2.9 Ga may be similar to the modern continental arc, and thus the plate tectonics in the Yangtze Craton probably commenced before 2.9 Ga.

5.1.2. Late granitic-dominated magmatic stage

5.1.2.1. 2.8 Ga biotite-granitic magmatism. The oldest emplacement age (2.81 Ga; KH258) of the 2.8 Ga biotite-granites overlaps the detrital zircon ages (ca. 2.82 Ga) from Archean sandstones in the Huji area (Fig. 1a) (Z.J. Wang et al., 2013a), while the youngest age (2.78 Ga; KH229) resembles the protolith age (ca. 2.77 Ga) of Huangtuling granulites in the North Dabie orogen (Wu et al., 2008). It means that the 2.8 Ga magmatism might be common in the Yangtze Craton.

The geochemical features of the 2.8 Ga granites significantly differ from those of the 3.3–2.9 Ga TTGs (Fig. 12). Their major element

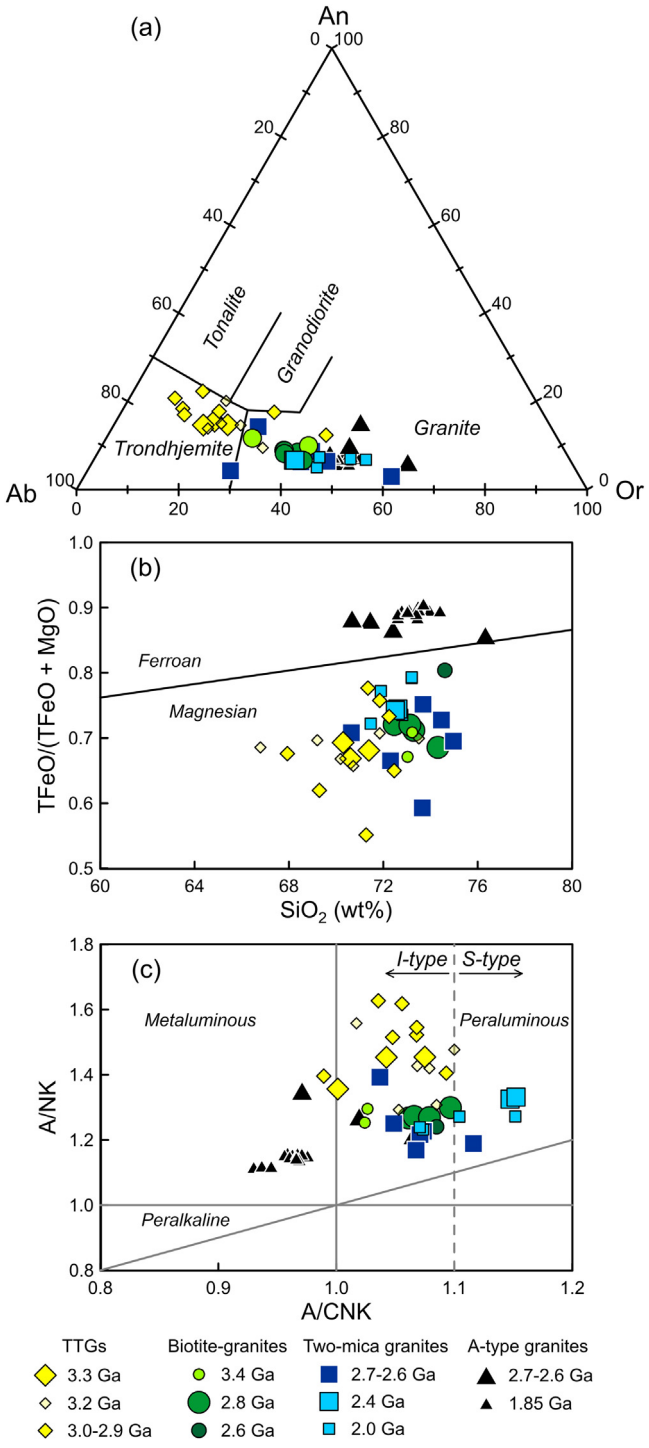

Fig. 7. (a) Classification of gneissic granitoids from the Kongling Terrane by normative feldspar compositions (Barker, 1979). (b) SiO_2 vs. TFeO/(TFeO + MgO) diagram (after Frost et al., 2001). (c) A/NK vs. A/CNK diagram (modified from Maniar and Piccoli, 1989). Symbols: diamonds, TTGs; circles, biotite-granites; squares, two-mica granites; triangles, A-type granites. Data sources include this and previous studies (Gao et al., 1999, 2011; Xiong et al., 2009; Peng et al., 2012; Chen et al., 2013; Guo et al., 2014b; Li et al., 2014; Y.B. Wu's unpublished data).

compositions are consistent with partial melts from tonalites as determined by experimental studies, rather than metabasalts as for the older TTGs (Fig. 11). Their low contents of Fe-Mg minerals (<1% biotite), TFe_2O_3 + MgO (0.89–1.61 wt%), and total REEs (45–67 ppm) require fractionation of REE-bearing ferromagnesian minerals (e.g., amphibole or pyroxene) (Figs. 2b, c, and 9h; Table 3). Because amphibole preferentially incorporates middle REEs, its fractionation would cause middle REE depletion in the residue melt (Nicholls and Harris, 1980; Sisson, 1994; Chazot et al., 1996), as observed in sample KH229 (Fig. 9h). A possible explanation for the genesis of 2.8 Ga magmatism would be melting of diorite/tonalite by a reaction such as plagioclase + biotite = amphibole + melt (e.g., Sisson et al., 2005; Watkins et al., 2007). This would reconcile both the fractionation of amphibole and the absence of Eu anomalies (Eu/Eu^* 1.12–1.29), considering that plagioclase contributes largely to the melt formation (e.g., Sisson et al., 2005; Watkins et al., 2007). However, amphibole is absent in these 2.8 Ga biotite-granites, which leaves the fractionation of amphibole still an open question.

5.1.2.2. 2.7–2.6 Ga biotite- and two-mica granitic magmatism. The 2.7–2.6 Ga magnesian granites in this study include biotite-granite KH233 (2.66 Ga) and two-mica granites KH196 (2.70 Ga), KH216 (2.64 Ga), and KH199 (2.64 Ga) (Figs. 4g–j). They show similar chemical compositions (Figs. 9i and j), which are also comparable to two 2.7 Ga gneissic two-mica granites KH163 and KH184 (2.71 Ga and 2.69 Ga, respectively) from the eastern North Kongling Terrane (Chen et al., 2013). These biotite or two-mica granites are all magnesian, chemically different from the 2.67–2.62 Ga A-type granites (ferroan) in the same region (Chen et al., 2013) (Figs. 7b and 8).

Compared to the older granitoids, the 2.7–2.6 Ga magnesian granites have a more heterogeneous source. Their major element compositions mainly resemble partial melts of tonalitic sources, but two of them indicate mafic and metasedimentary sources, respectively (Fig. 11). The contribution from metasediments is also favored by the high K_2O content (up to 6.71 wt%), high A/CNK (up to 1.12), and the presence of primary muscovite in the two-mica granites (Fig. 2d). The variable mean $\varepsilon_{Hf}(t)$ values (−4.9 to 0.9) and T_{DM2} (3.29–3.03 Ga) in these 2.7–2.6 Ga magnesian granites indicate that their source regions may be heterogeneous, consisting of both juvenile and relatively ancient components (Figs. 6e, f, and 13; Supplementary Table S3). Two samples (KH233 and KH196) contain minor 3.4–3.1 Ga inherited zircon ages, which seems to suggest that the local 3.4–3.1 Ga gneisses might represent the relatively ancient components in the source region. However, melting of the 3.4–3.1 Ga gneisses to generate the 2.7–2.6 Ga magmas would require either (1) these gneisses to have $^{176}Lu/^{177}Hf$ >0.02 (Fig. 13), which is very unlikely considering that they are felsic rocks, or (2) admixing of depleted mantle materials. Nevertheless, these 2.7–2.6 Ga magnesian granites have very high SiO_2 contents (73.65–74.46 wt%) and low MgO (0.18–0.50 wt%), Cr (0.58–3.08 ppm) and Ni (2.14–5.56 ppm) contents (Table 3), which rules out the involvement of the mantle or mantle-derived materials in their origin, even for the sample with the highest $\varepsilon_{Hf}(t)$ values. Two scenarios could explain such contradictions. One plausible scenario is the "zircon effect" during anatexis of the 3.4–3.1 Ga gneisses (e.g., Zeh et al., 2009, 2011). Residual zircons in the source may retain a significant amount of ^{177}Hf at the source, resulting in heterogeneous Hf isotopic compositions in magmatic zircons of granitic rocks, which may not necessarily indicate magma mixing of multiple sources (Tang et al., 2014). The other scenario is melting of a younger (<3.1 Ga) juvenile crust, under which circumstance the 3.4–3.1 Ga zircons could be explained as xenocrysts. This juvenile crust, however, is unlikely to be the 3.0–2.9 Ga TTG rocks discussed above. Because as shown in Fig. 13, these rocks are not juvenile at all (showing predominant negative $\varepsilon_{Hf}(t)$ values), and would have had essentially subchondritic ε_{Hf} values at 2.7 Ga. Instead, the juvenile crust might be the mafic crust formed <3.1 Ga, as inferred from (1) the mafic enclaves and dykes with island arc affinities hosted in the 3.0–2.9 Ga (Wei and Wang, 2012; Wei and Jing, 2013; Li et al., 2014), and (2) 2.86 Ga amphibolite with radiogenic Hf isotopic compositions ($\varepsilon_{Hf}(t)$ values up to 5.6) from the North Kongling Terrane (Wu et al., 2009). However, melting of such juvenile mafic crust

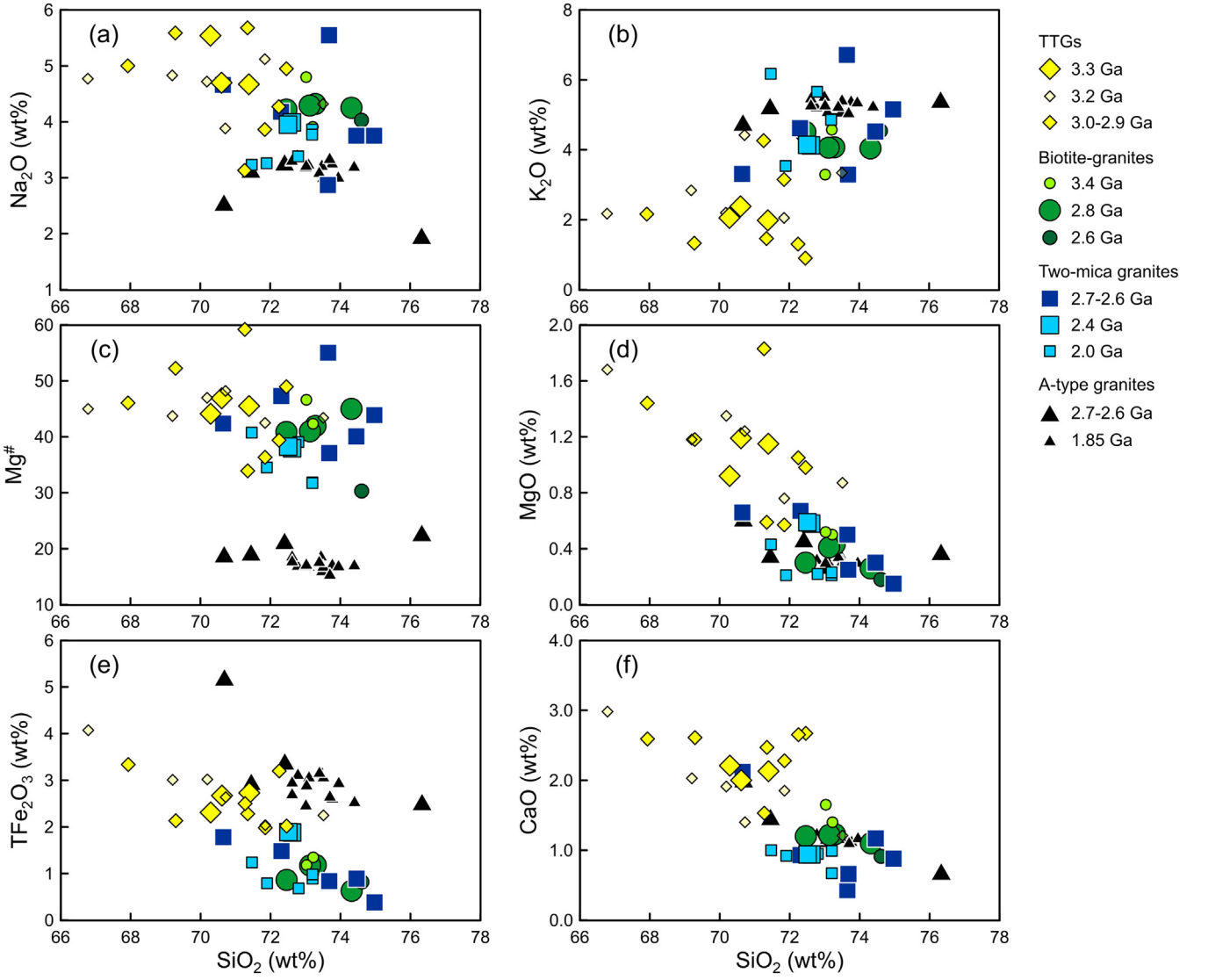

Fig. 8. Harker diagrams of gneissic granitoids from the Kongling Terrane, showing SiO_2 vs. (a) Na_2O, (b) K_2O, (c) $Mg^{\#}$, (d) MgO, (e) TFe_2O_3, and (f) CaO. Symbols: diamonds, TTGs; circles, biotite-granites; squares, two-mica granites; triangles, A-type granites. Data sources include this and previous studies (Gao et al., 1999, 2011; Xiong et al., 2009; Peng et al., 2012; Chen et al., 2013; Guo et al., 2014b; Li et al., 2014; Y.B. Wu's unpublished data).

would produce melts with different compositions from the majority of the 2.7–2.6 Ga magnesian granites. Thus, this scenario could only explain a small proportion of these granites (Fig. 13).

Therefore, the 2.7–2.6 Ga biotite- and two-mica granites are likely to have been produced by reworking of a heterogeneous source region (consisting of 3.4–3.1 Ga granitoid gneisses as well as minor 3.0–2.9 Ga mafic rocks and metasediments), and their formation may have been affected by the retention of residual zircon during melting.

5.1.2.3. 2.4 Ga two-mica granitic magmatism. Two amphibole leptynites from the North Kongling Terrane gave identical TIMS zircon U–Pb discordia ages of ca. 2.43 Ga (Zheng et al., 1991; Ma et al., 1997). In this study, the two-mica granite KH234 yields a similar emplacement age (2.42 Ga) (Fig. 4k), which verifies the existence of 2.4 Ga magmatism in the Yangtze Craton. The presence of muscovite (Fig. 2e) and high A/CNK (1.15) (Fig. 7c) of KH234 suggest that sediments may have been involved in its formation. The magmatic zircons show negative $\varepsilon_{Hf}(t)$ (mean -11.2 ± 0.9) and Paleoarchean T_{DM2} (mean 3.42 ± 0.04) (Figs. 6g and h), indicating reworking of ancient basement rocks in the Kongling Terrane.

Although 2.4 Ga rocks have only been reported from the Kongling Terrane, coeval detrital zircons have been widely reported from the Yangtze Craton (X.M. Liu et al., 2008; L.J. Wang et al., 2013; Zheng et al., 2013; Cui et al., 2014). Their $\varepsilon_{Hf}(t)$ values vary largely from −14 to 10 (Fig. 13) suggesting juvenile crustal growth in addition to crustal reworking in the Yangtze Craton.

5.1.2.4. 2.0 Ga two-mica granitic magmatism. Two-mica granite KH231 has minor muscovite (Fig. 2f) and high A/CNK (1.10) (Fig. 7c), and falls into the field of partial melts from metasediments as determined by experimental studies (Fig. 11). It implies that this sample may be S-type in nature. This is consistent with the observation that the Kongling Terrane preserves voluminous syn-collisional S-type granites and migmatites (Yin et al., 2013; Li et al., 2014). The unradiogenic zircon Hf isotopic compositions (mean $\varepsilon_{Hf}(t)$ -12.9 ± 0.4 and T_{DM2} 3.15 ± 0.02 Ga) of magmatic zircons in sample KH231 indicate anatexis of ancient felsic crust (Fig. 6i). As shown in Fig. 13, the age-$\varepsilon_{Hf}(t)$ data of these magmatic zircons fall into the evolutionary trend of the 2.7 Ga magnesian granites. This suggests that the sedimentary source rocks for the 2.0 Ga granitic magmatism may have sourced dominantly from local 2.7 Ga magnesian granites.

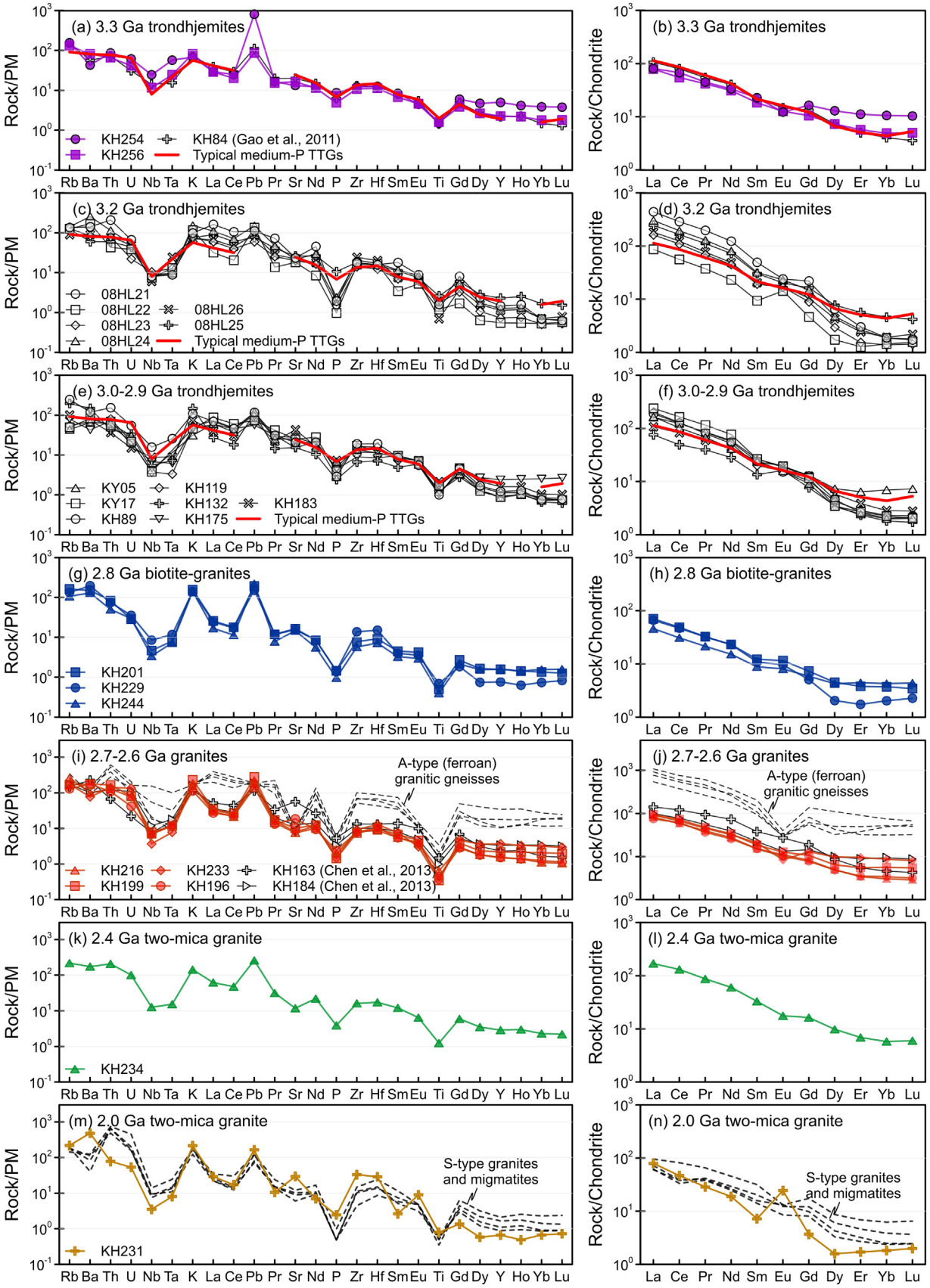

Fig. 9. Primitive mantle (PM)-normalized spidergrams (left panel) and chondrite-normalized REE patterns (right panel) for gneissic granitoids from the Kongling Terrane. The solid lines with filled symbols represent samples from this study, while the dashed lines with empty symbols denote those from previous studies, including 3.3 Ga trondhjemites (Gao et al., 2011), 3.2 Ga trondhjemites (Jiao et al., 2009; Y.B. Wu's unpublished data), 3.0–2.9 Ga trondhjemites (Gao et al., 1999, 2011; Chen et al., 2013), 2.7–2.6 Ga A-type (ferroan) granites (Chen et al., 2013), and 2.0 Ga S-type granites and migmatites (Li et al., 2014). The thick lines in (a)–(f) indicate the typical medium-HREE or medium-pressure TTGs that formed under garnet-amphibolite facies (Moyen and Martin, 2012). PM and chondrite values are taken from McDonough and Sun (1995).

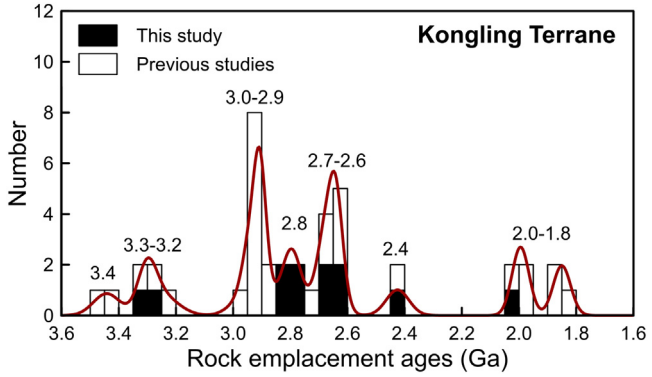

Fig. 10. Kernel density estimate (Vermeesch, 2012) and histogram of the emplacement ages of granitoid rocks from the Kongling Terrane. The filled and empty bars represent data from this and previous studies, respectively (Qiu et al., 2000; Zhang et al., 2006a; Jiao et al., 2009; Xiong et al., 2009; Gao et al., 2011; Peng et al., 2012; Chen et al., 2013; Yin et al., 2013; Guo et al., 2014b; Li et al., 2014).

5.2. Tectonic significance of the TTG-granite transition at 2.8 Ga in the Kongling Terrane

Multiple generations of Paleoarchean-Paleoproterozoic granitoid rocks from the Kongling Terrane in the Yangtze Craton could define an early TTG stage (3.3–2.9 Ga) and a late granite stage (2.8–2.0 Ga). A dramatic change is observed at 2.8 Ga in mineralogy, geochemistry, and petrogenesis of the granitoid magmatism, from Na-rich trondhjemites to K-rich granites (Figs. 12 and 14). The geochemical features of the 3.3–2.9 Ga TTGs suggest that they may have been commonly derived from low-K metabasalts, but at different depths with/without melt–mantle interactions (Figs. 9, 11, and 12). In fact, the 3.3 and 3.2 Ga trondhjemites suggest melting of mafic rocks at increasing pressures, as indicated by

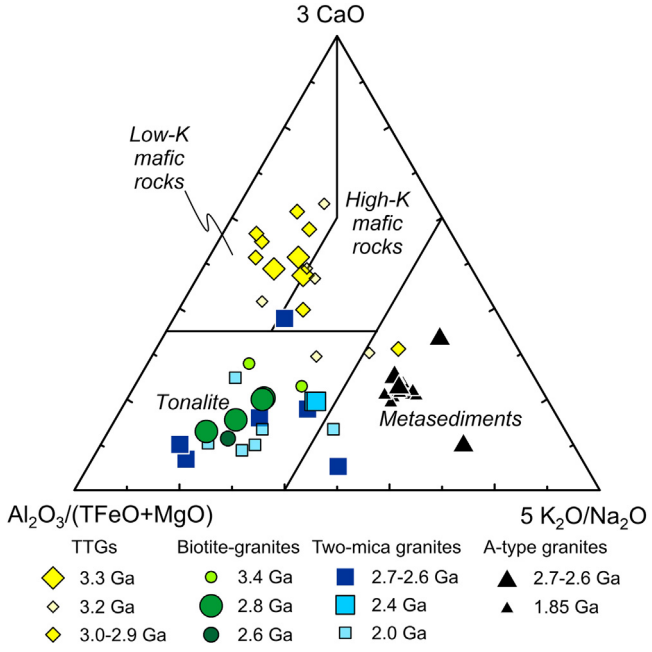

Fig. 11. Ternary diagram of $Al_2O_3/(TFeO + MgO)–3CaO–5(K_2O/Na_2O)$ (after Laurent et al., 2014). The different fields represent the composition of melts derived from a range of potential sources (tonalites, metasediments, low- and high-K mafic rocks), determined by the major-element compositions of partial melts from experimental studies (see references in Laurent et al., 2014). Symbols: diamonds, TTGs; circles, biotite-granites; squares, two-mica granites; triangles, A-type granites. Data sources include this and previous studies (Gao et al., 1999, 2011; Xiong et al., 2009; Peng et al., 2012; Chen et al., 2013; Guo et al., 2014b; Li et al., 2014; Y.B. Wu's unpublished data).

the rising La_N/Yb_N ratio from 3.3 to 3.2 Ga (Fig. 12h). This could be explained by progressive thickening and concomitant differentiation of a thickened mafic crust, for instance, an oceanic plateau in an intraplate environment (Moyen and Martin, 2012). In contrast, the 3.0–2.9 Ga high-pressure TTGs clearly show evidence for mantle–melt interactions (high Cr and Ni contents together with minor depleted mantle-like $\varepsilon_{Hf}(t)$ values), which is more consistent with a subduction origin, e.g., a continental arc setting, as discussed above (e.g., Smithies, 2000; Martin and Moyen, 2002; Martin et al., 2005; Moyen and Martin, 2012). This suggests that the maximum unequivocal age for a plate tectonics behavior in the Yangtze craton is 3.0–2.9 Ga.

In contrast, the younger biotite- and two-mica granites (2.8, 2.7–2.6, 2.4, and 2.0 Ga) were probably formed by repeated anatexis of pre-existing basement rocks (TTGs and/or metasediments) (e.g., Yin et al., 2013). The introduction of both metasediments and juvenile mantle-derived components into the magma sources seems to have started since 2.7–2.6 Ga (Figs. 11 and 13). The petrogenesis of the 2.8–2.0 Ga granites may be related to multiple collisional events (as discussed in Section 5.1), implying a change in geodynamics from (1) pre-2.8 Ga reworking of pre-existing mafic crust by crustal thickening or subduction to (2) post-2.8 Ga reworking of more felsic ancient crust by collisions and subsequent crustal extension (e.g., Yin et al., 2013; Li et al., 2014 for the 2.0 Ga S-type granites).

An important significance of the TTG-granite transition is to increase the stability of the continental crust and its underlying lithospheric mantle. Since granites are rich in incompatible and radioactive heat-producing elements (K, U, and Th), repeated granitic magmatism (especially during the 2.7–2.6 Ga) by crustal anatexis would transfer these elements from deep lithosphere to shallow depths, facilitating the maturation and stabilization of the continental crust (Korhonen and Johnson, 2015; Zhou et al., 2015). The stabilization of the lithospheric mantle was assisted by the emplacement of highly fertile mantle-derived 2.67–2.62 Ga A-type granitic magmas (Chen et al., 2013). Therefore, the TTG-granite transition also means that the stabilization of the Yangtze Craton may have initiated since 2.8 Ga and peaked at 2.7–2.6 Ga. After 2.6 Ga, juvenile crustal growth in the Yangtze Craton has been limited (Fig. 13). However, the final cratonization of the Yangtze Craton had not been accomplished until 1.85 Ga, as marked by the emplacement of 1.85 Ga A-type granites in the North Kongling Terrane (Xiong et al., 2009; Peng et al., 2012).

In a global view, similar TTG-granite and tectonic transitions have been widely recognized in other Archean cratons (e.g., Superior, Amazonian, Karelian, Kaapvaal, Pilbara, Dharwar, and North China) (Laurent et al., 2014 and references therein). Such transitions usually include two distinct stages: a long period (0.2–0.5 Ga) of TTG emplacement, followed by a shorter period (0.02–0.15 Ga) of granitoid (biotite-granite, two-mica granite, and sanukitoid) emplacement (Moyen et al., 2003; Moyen and Martin, 2012; Laurent et al., 2014). This two-stage evolution pattern of Archean granitoid magmatism may indicate the commencement of the first global subduction–collision cycle in the Earth's history, as a consequence of the Earth's cooling (Martin and Moyen, 2002; Moyen et al., 2003; Condie, 2005b; Martin et al., 2005; Moyen and Martin, 2012; Laurent et al., 2014). The transition at 2.8 Ga in the Kongling Terrane, Yangtze Craton (Fig. 14) is later than the Pilbara (2.95 Ga) and Amazonia (2.85 Ga) Cratons, similar to the Kaapvaal Craton (2.85–2.70 Ga), but earlier than the Dharwar (2.55 Ga) and North China (2.55–2.45 Ga) Cratons (e.g., Smithies and Champion, 2000; Moyen et al., 2003; Van Kranendonk et al., 2007; Almeida et al., 2010; Zhai and Santosh, 2011; Zhao and Cawood, 2012; Laurent et al., 2014). However, Neoarchean sanukitoid have not been found from the Yangtze Craton yet. The Kongling Terrane may have a continental arc setting during 3.0–2.9 Ga, and later it experienced protracted intracrustal differentiation from 2.8 to 2.0 Ga, which

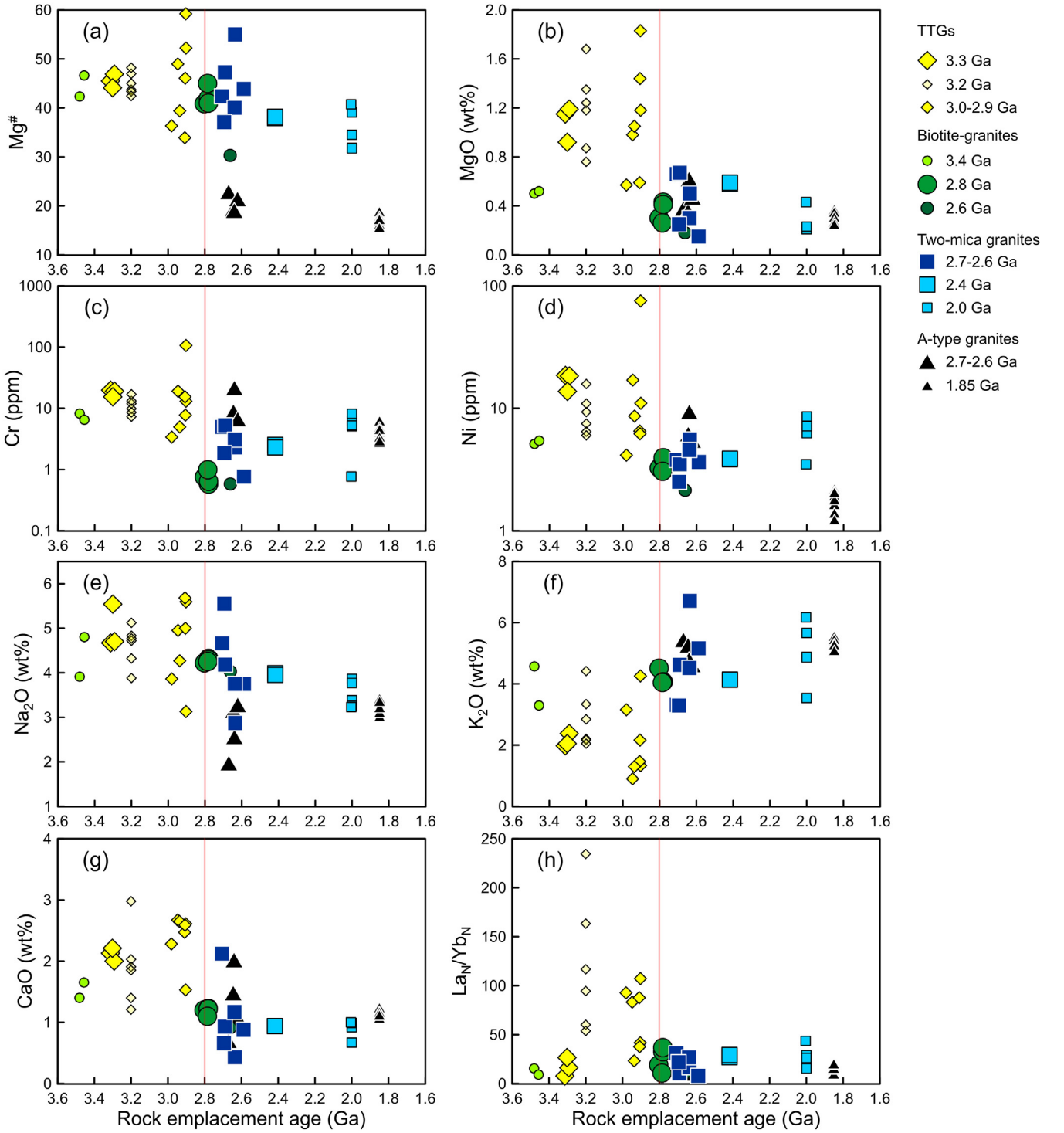

Fig. 12. Emplacement ages vs. major element contents or element ratios for granitoid rocks from the Kongling Terrane: (a) $Mg^{\#}$, (b) MgO, (c) Cr, (d) Ni, (e) Na_2O, (f) K_2O, (g) CaO, and (h) La_N/Yb_N. Symbols: diamonds, TTGs; circles, biotite-granites; squares, two-mica granites; triangles, A-type granites. Data sources include this and previous studies (Gao et al., 1999, 2011; Xiong et al., 2009; Peng et al., 2012; Chen et al., 2013; Guo et al., 2014b; Li et al., 2014; Y.B. Wu's unpublished data).

might not be a tectonic setting suitable for the generation of sanukitoids (Laurent et al., 2014 and references therein).

5.3. Significance of the 2.7–2.6 Ga magmatic-metamorphic events in the Yangtze Craton

2.7 Ga magmatism has been widely recorded in most of the Archean cratons worldwide (cf., Condie et al., 2009). This global magmatism was attributed either to a mantle plume (Condie, 1998, 2005a; Wyman, 2003; Condie and O'Neill, 2010; Said et al., 2010), or to subduction, accretion, and collision events related to supercontinent amalgamation (Aspler and Chiarenzelli, 1998; Campbell and Allen, 2008; Condie and Aster, 2010; Bradley, 2011). Vast amounts of TTGs and/or voluminous syn- or post-collisional granites could be produced/preserved during the amalgamation of supercontinent (e.g., Polat et al., 1998; Polat and Kerrich, 2002; Condie et al., 2009; Jiang et al., 2010; Zeh et al., 2010; Manikyamba and Kerrich, 2012; Zhu et al., 2013; Wan et al., 2014).

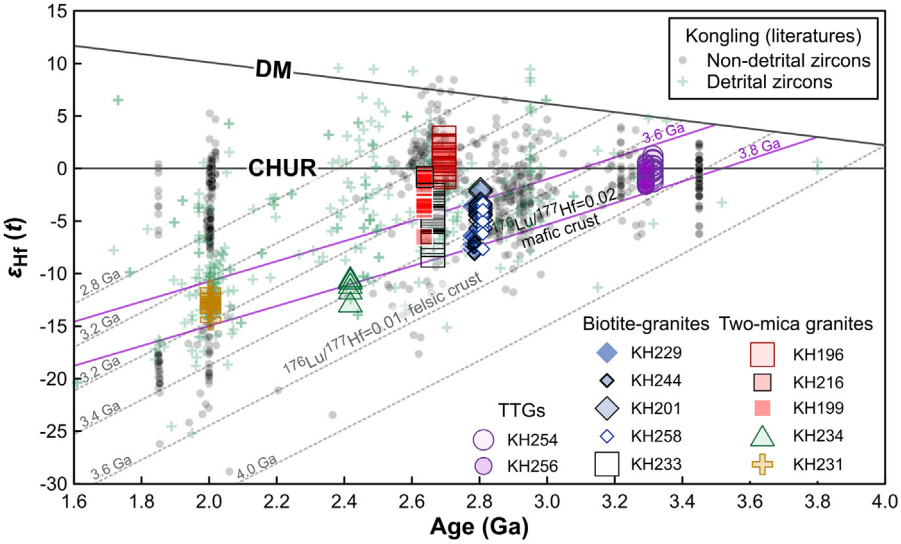

Fig. 13. Zircon $\varepsilon_{Hf}(t)$ values vs. crystallization ages for gneissic granitoids from the Kongling Terrane. The small circles and crosses represent non-detrital zircons (Zhang et al., 2006a, b; Zheng et al., 2006; Jiao et al., 2009; Peng et al., 2009, 2012; Wu et al., 2009; Xiong et al., 2009; Gao et al., 2011; Wei and Wang, 2012; Chen et al., 2013; Guo et al., 2014b; Li et al., 2014) and detrital zircons (Zhang et al., 2006c; X.M. Liu et al., 2008; Gao et al., 2011; L.J. Wang et al., 2013; Yin et al., 2013; Cui et al., 2014) with age concordance between 98% and 102% from the Kongling Terrane, respectively. The solid and dashed lines indicate the evolution trends of a mafic crust ($^{176}Lu/^{177}Hf = 0.02$) (Zeh et al., 2014) and a felsic crust ($^{176}Lu/^{177}Hf = 0.01$), respectively. The depleted mantle (DM) evolution line is from Blichert-Toft and Puchtel (2010). *Abbreviation*: CHUR, chondritic uniform reservoir.

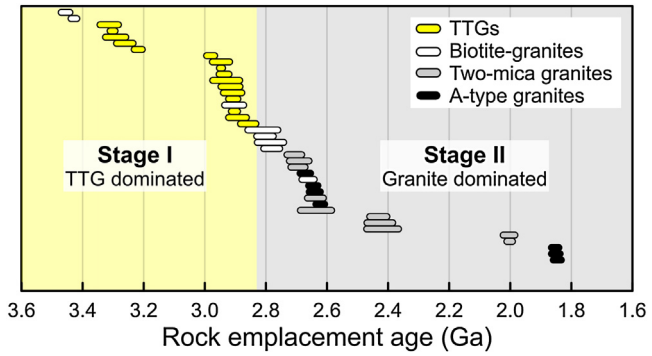

Fig. 14. Emplacement ages of the Paleoarchean-Paleoproterozoic granitoid rocks from the Kongling Terrane. Data sources include this and previous studies (Zheng et al., 1991; Ma et al., 1997; Zhang et al., 2006a; Zheng et al., 2006; Jiao et al., 2009; Xiong et al., 2009; Gao et al., 2011; Peng et al., 2012; Chen et al., 2013; Yin et al., 2013; Guo et al., 2014b; Li et al., 2014). The bar widths are given at 2σ level.

In the Yangtze Craton, the 2.7–2.6 Ga granitic magmatism is widespread at least in the central and the northern parts, e.g., Kongling, Huji, Huangtuling, Yudongzi, Jingshan, Zhenyuan, and Ningxiang (Zhang et al., 2001; Zheng et al., 2006; Sun et al., 2008; Wu et al., 2008; Z.J. Wang et al., 2013a, b; Zhou et al., 2015) (Fig. 1c). However, neither coeval mafic-ultramafic rocks nor TTGs have been found in the Yangtze Craton. Besides, the unradiogenic Hf isotopic compositions of the 2.7–2.6 Ga granites and xenocrystic zircons indicate that crustal reworking might be dominant during the 2.7–2.6 Ga magmatism in the Yangtze Craton (this study; Zheng et al., 2006; Chen et al., 2013; Zhou et al., 2015) (Fig. 13). These observations fit an orogenic setting instead of a plume or a subduction setting. Moreover, 2.75–2.72 Ga high-grade metamorphism has been preserved in orthogneisses, amphibolites, and metapelites from the Kongling Terrane (Ling et al., 1998; Qiu et al., 2000; Jiao et al., 2009; Wei and Wang, 2012). Its age is slightly earlier than the 2.71–2.64 Ga biotite- and two-mica granites as well as the 2.67–2.62 Ga A-type granites in the Kongling Terrane. Thus, we propose a two-stage model to explain the 2.7–2.6 Ga metamorphism and magmatism: (1) an early collisional stage (2.75–2.72 Ga), which is represented by the 2.75–2.72 Ga high-grade metamorphism, and (2) a late extensional stage (2.71–2.62 Ga), which might be related to collapse of orogenic root and subsequent crustal extension and mantle upwelling, generating the 2.71–2.64 Ga biotite- and two-mica granitic magmatism and the 2.67–2.62 Ga A-type granitic magmatism. It is interesting that the timing (2.75–2.72 Ga) of this early collisional stage is consistent with a 2.7 Ga global orogeny, as recorded in the Limpopo Belt from southern Africa, which jointed the Kaapvaal and Zimbabwe cratons together at 2.72 Ga (Zeh et al., 2009; Kramers and Mouri, 2011; Laurent et al., 2014). This global orogeny was suggested to have formed the probably earliest supercontinent Kenorland (Rämö et al., 2005; Bradley, 2011). We tentatively propose that the 2.7–2.6 Ga metamorphic and magmatic events in the Yangtze Craton may be related to this 2.7 Ga global orogeny as well. Admittedly, more geochemical and high-precision geochronological works are needed in future to test this hypothesis.

6. Conclusions

We studied the whole-rock element and zircon U–Pb–Lu–Hf isotopic compositions of twelve gneissic granitoids from the Kongling Terrane, Yangtze Craton. The following conclusions were obtained:

1. The 3.3 Ga trondhjemites confirm the existence of 3.3 Ga trondhjemitic magmatism in the Yangtze Craton. Their major and trace element compositions suggest that they were derived from amphibolite-facies low-K mafic crust.
2. The younger granites (2.8, 2.7–2.6, 2.4, and 2.0 Ga) are basically leucogranitic. Their major element compositions, inherited zircon ages, and magmatic zircon Hf isotopic features suggest that they were mainly produced by repeated anatexis of ancient basement rocks (TTGs and/or metasediments) in the Kongling Terrane.
3. The Paleoarchean-Paleoproterozoic granitoid magmatism (3.3–3.2, 3.0–2.9, 2.8, 2.7–2.6, 2.4, and 2.0 Ga) in the Kongling Terrane shows a remarkable change in petrology, geochemistry, and petrogenesis at 2.8 Ga. This may reflect a change in the geodynamics from (1) pre-2.8 Ga reworking of pre-existing mafic crust by crustal thickening or subduction to

(2) post-2.8 Ga reworking of more felsic ancient crust by collisions and subsequent crustal extension.

4. A two-stage model is proposed to explain the 2.7–2.6 Ga metamorphic and magmatic events in the Yangtze Craton: (1) an early collisional stage, represented by the 2.75–2.72 Ga high-grade metamorphism, and (2) a late extensional stage, during which the 2.71–2.64 Ga biotite- and two-mica granites and the 2.67–2.62 Ga A-type granites were produced by orogenic root collapse and subsequent mantle upwelling. The 2.7–2.6 Ga metamorphic and magmatic events in the Yangtze Craton may be related to the 2.7 Ga global orogeny.

Acknowledgements

We would like to thank Jian-Qi Wang for whole-rock major element analysis and colleges from the GPMR Lab for assistance in zircon U–Pb–Lu–Hf analysis. We are grateful to Oscar Laurent and one anonymous reviewer for their constructive suggestions that have significantly improved both the quality and the clarity of the manuscript. This research was supported by the National Natural Science Foundation of China (41502049, 41170316 and 41373026) and Chinese Ministry of Education (B07039), the Fundamental Research Funds for National Universities, as well as special funds from the State Key Laboratory of Geological Processes and Mineral Resources and from the State Key Laboratory of Continental Dynamics.

Appendix A. Supplementary data

Supplementary data associated with this article can be found, in the online version, at http://dx.doi.org/10.1016/j.precamres.2015.09.007.

References

Almeida, J.d.A.C., Dall'Agnol, R., Dias, S.B., Althoff, F.J., 2010. Origin of the Archean leucogranodiorite–granite suites: evidence from the Rio Maria terrane and implications for granite magmatism in the Archean. Lithos 120, 235–257.
Amelin, Y., Lee, D.C., Halliday, A.N., 2000. Early-middle archaean crustal evolution deduced from Lu–Hf and U–Pb isotopic studies of single zircon grains. Geochim. Cosmochim. Acta 64, 4205–4225.
Andersen, T., 2002. Correction of common lead in U–Pb analyses that do not report ^{204}Pb. Chem. Geol. 192, 59–79.
Armstrong, R.L., Harmon, R.S., 1981. Radiogenic isotopes: the case for crustal recycling on a near-steady-state no-continental-growth earth [and discussion]. Philos. Trans. R. Soc. Lond. Ser. A: Math. Phys. Sci. 301, 443–472.
Aspler, L.B., Chiarenzelli, J.R., 1998. Two Neoarchean supercontinents? Evidence from the Paleoproterozoic. Sediment. Geol. 120, 75–104.
Barker, F., 1979. Trondhjemite: definition, environment and hypotheses of origin. In: Barker, F. (Ed.), Trondhjemites, Dacites and Related Rocks. Elsevier, Amsterdam, pp. 1–12.
Belousova, E.A., Kostitsyn, Y.A., Griffin, W.L., Begg, G.C., O'Reilly, S.Y., Pearson, N.J., 2010. The growth of the continental crust: constraints from zircon Hf-isotope data. Lithos 119, 457–466.
Blichert-Toft, J., 2008. The Hf isotopic composition of zircon reference material 91500. Chem. Geol. 253, 252–257.
Blichert-Toft, J., Chauvel, C., Albarède, F., 1997. Separation of Hf and Lu for high-precision isotope analysis of rock samples by magnetic sector-multiple collector ICP-MS. Contrib. Mineral. Petrol. 127, 248–260.
Blichert-Toft, J., Puchtel, I.S., 2010. Depleted mantle sources through time: evidence from Lu–Hf and Sm–Nd isotope systematics of Archean komatiites. Earth Planet. Sci. Lett. 297, 598–606.
Bouvier, A., Vervoort, J.D., Patchett, P.J., 2008. The Lu–Hf and Sm–Nd isotopic composition of CHUR: constraints from unequilibrated chondrites and implications for the bulk composition of terrestrial planets. Earth Planet. Sci. Lett. 273, 48–57.
Bradley, D.C., 2008. Passive margins through earth history. Earth Sci. Rev. 91, 1–26.
Bradley, D.C., 2011. Secular trends in the geologic record and the supercontinent cycle. Earth Sci. Rev. 108, 16–33.
Campbell, I.H., Allen, C.M., 2008. Formation of supercontinents linked to increases in atmospheric oxygen. Nat. Geosci. 1, 554–558.
Chazot, G., Menzies, M.A., Harte, B., 1996. Determination of partition coefficients between apatite, clinopyroxene, amphibole, and melt in natural spinel lherzolites from Yemen: implications for wet melting of the lithospheric mantle. Geochim. Cosmochim. Acta 60, 423–437.
Chen, K., Gao, S., Wu, Y.B., Guo, J.L., Hu, Z.C., Liu, Y.S., Zong, K.Q., Liang, Z.W., Geng, X.L., 2013. 2.6–2.7 Ga crustal growth in Yangtze craton, South China. Precambrian Res. 224, 472–490.
Chen, R.X., Zheng, Y.F., Xie, L., 2010. Metamorphic growth and recrystallization of zircon: distinction by simultaneous in-situ analyses of trace elements, U–Th–Pb and Lu–Hf isotopes in zircons from eclogite-facies rocks in the Sulu orogen. Lithos 114, 132–154.
Collerson, K.D., Kamber, B.S., 1999. Evolution of the continents and the atmosphere inferred from Th–U–Nb systematics of the depleted mantle. Science 283, 1519–1522.
Condie, K.C., 1998. Episodic continental growth and supercontinents: a mantle avalanche connection? Earth Planet. Sci. Lett. 163, 97–108.
Condie, K.C., 2005a. High field strength element ratios in Archean basalts: a window to evolving sources of mantle plumes? Lithos 79, 491–504.
Condie, K.C., 2005b. TTGs and adakites: are they both slab melts? Lithos 80, 33–44.
Condie, K.C., 2014. Growth of continental crust: a balance between preservation and recycling. Mineral. Mag. 78, 623–637.
Condie, K.C., Aster, R.C., 2010. Episodic zircon age spectra of orogenic granitoids: the supercontinent connection and continental growth. Precambrian Res. 180, 227–236.
Condie, K.C., Belousova, E., Griffin, W.L., Sircombe, K.N., 2009. Granitoid events in space and time: constraints from igneous and detrital zircon age spectra. Gondwana Res. 15, 228–242.
Condie, K.C., O'Neill, C., 2010. The Archean-Proterozoic boundary: 500 my of tectonic transition in Earth history. Am. J. Sci. 310, 775–790.
Cui, X., Zhu, W.B., Ge, R.F., 2014. Provenance and crustal evolution of the Northern Yangtze Block revealed by detrital zircons from Neoproterozoic–Early Paleozoic sedimentary rocks in the Yangtze Gorges Area, South China. J. Geol. 122, 217–235.
Dhuime, B., Hawkesworth, C.J., Cawood, P.A., Storey, C.D., 2012. A change in the geodynamics of continental growth 3 billion years ago. Science 335, 1334–1336.
Dong, S.W., Zhang, Y.Q., Gao, R., Su, J.B., Liu, M., Li, J.H., 2015. A possible buried Paleoproterozoic collisional orogen beneath central South China: evidence from seismic-reflection profiling. Precambrian Res. 264, 1–10.
Drummond, M.S., Defant, M.J., 1990. A model for trondhjemite-tonalite-dacite genesis and crustal growth via slab melting: Archean to modern comparisons. J. Geophys. Res. Solid Earth 95, 21503–21521.
Ducea, M.N., Saleeby, J.B., Bergantz, G., 2015. The architecture, chemistry, and evolution of continental magmatic arcs. Annu. Rev. Earth Planet. Sci. 43, 299–331.
Eggins, S.M., Kinsley, L.P.J., Shelley, J.M.G., 1998. Deposition and element fractionation processes during atmospheric pressure laser sampling for analysis by ICP-MS. Appl. Surf. Sci. 127–129, 278–286.
Ernst, W.G., 2009. Archean plate tectonics, rise of Proterozoic supercontinentality and onset of regional, episodic stagnant-lid behavior. Gondwana Res. 15, 243–253.
Fisher, C.M., Hanchar, J.M., Samson, S.D., Dhuime, B., Blichert-Toft, J., Vervoort, J.D., Lam, R., 2011. Synthetic zircon doped with hafnium and rare earth elements: a reference material for in situ hafnium isotope analysis. Chem. Geol. 286, 32–47.
Fisher, C.M., Vervoort, J.D., Hanchar, J.M., 2014. Guidelines for reporting zircon Hf isotopic data by LA-MC-ICPMS and potential pitfalls in the interpretation of these data. Chem. Geol. 363, 125–133.
Frost, B.R., Barnes, C.G., Collins, W.J., Arculus, R.J., Ellis, D.J., Frost, C.D., 2001. A geochemical classification for granitic rocks. J. Petrol. 42, 2033–2048.
Furnes, H., Banerjee, N.R., Muehlenbachs, K., Staudigel, H., de Wit, M., 2004. Early life recorded in Archean pillow lavas. Science 304, 578–581.
Gao, S., Ling, W.L., Qiu, Y.M., Lian, Z., Hartmann, G., Simon, K., 1999. Contrasting geochemical and Sm–Nd isotopic compositions of Archean metasediments from the Kongling high-grade terrain of the Yangtze craton: evidence for cratonic evolution and redistribution of REE during crustal anatexis. Geochim. Cosmochim. Acta 63, 2071–2088.
Gao, S., Yang, J., Zhou, L., Li, M., Hu, Z.C., Guo, J.L., Yuan, H.L., Gong, H.J., Xiao, G.Q., Wei, J.Q., 2011. Age and growth of the Archean Kongling Terrain, South China, with emphasis on 3.3 Ga granitoid gneisses. Am. J. Sci. 311, 153–182.
Gao, S., Zhang, B.R., 1990. The discovery of Archean TTG gneisses in the northern Yangtze Platform and their implications. Earth Sci. J. China Univ. Geosci. 15, 675–679.
Gerdes, A., Zeh, A., 2009. Zircon formation versus zircon alteration – new insights from combined U–Pb and Lu–Hf in-situ LA-ICP-MS analyses, and consequences for the interpretation of Archean zircon from the Central Zone of the Limpopo Belt. Chem. Geol. 261, 230–243.
Guitreau, M., Blichert-Toft, J., Martin, H., Mojzsis, S.J., Albarède, F., 2012. Hafnium isotope evidence from Archean granitic rocks for deep-mantle origin of continental crust. Earth Planet. Sci. Lett. 337–338, 211–223.
Guo, J.L., Gao, S., Wu, Y.B., Hu, Z.C., Xu, W.L., Zong, K.Q., Liu, Y.S., Yuan, H.L., 2014a. Titanite evidence for Triassic thickened lower crust along southeastern margin of North China Craton. Lithos 206–207, 277–288.
Guo, J.L., Gao, S., Wu, Y.B., Li, M., Chen, K., Hu, Z.C., Liang, Z.W., Liu, Y.S., Zhou, L., Zong, K.Q., Zhang, W., Chen, H.H., 2014b. 3.45 Ga granitic gneisses from the Yangtze Craton, South China: implications for early Archean crustal growth. Precambrian Res. 242, 82–95.
Hawkesworth, C., Cawood, P., Dhuime, B., 2013. Continental growth and the crustal record. Tectonophysics 609, 651–660.
Hawkesworth, C.J., Dhuime, B., Pietranik, A.B., Cawood, P.A., Kemp, A.I.S., Storey, C.D., 2010. The generation and evolution of the continental crust. J. Geol. Soc. 167, 229–248.

Hoffmann, J.E., Münker, C., Næraa, T., Rosing, M.T., Herwartz, D., Garbe-Schönberg, D., Svahnberg, H., 2011. Mechanisms of Archean crust formation inferred from high-precision HFSE systematics in TTGs. Geochim. Cosmochim. Acta 75, 4157–4178.
Hu, J., Liu, X.C., Chen, L.Y., Qu, W., Li, H.K., Geng, J.Z., 2013. A ~2.5 Ga magmatic event at the northern margin of the Yangtze craton: evidence from U–Pb dating and Hf isotope analysis of zircons from the Douling Complex in the South Qinling orogen. Chin. Sci. Bull. 58, 3564–3579.
Hu, Z.C., Gao, S., Liu, Y.S., Hu, S.H., Chen, H.H., Yuan, H.L., 2008. Signal enhancement in laser ablation ICP-MS by addition of nitrogen in the central channel gas. J. Anal. At. Spectrom. 23, 1093–1101.
Hu, Z.C., Liu, Y.S., Gao, S., Liu, W.G., Zhang, W., Tong, X.R., Lin, L., Zong, K.Q., Li, M., Chen, H.H., Zhou, L., Yang, L., 2012. Improved in situ Hf isotope ratio analysis of zircon using newly designed X skimmer cone and jet sample cone in combination with the addition of nitrogen by laser ablation multiple collector ICP-MS. J. Anal. At. Spectrom. 27, 1391–1399.
Jackson, S.E., Pearson, N.J., Griffin, W.L., Belousova, E.A., 2004. The application of laser ablation-inductively coupled plasma-mass spectrometry to in situ U–Pb zircon geochronology. Chem. Geol. 211, 47–69.
Jahn, B.M., Wu, F.Y., Chen, B., 2000. Granitoids of the Central Asian Orogenic Belt and continental growth in the Phanerozoic. Geol. Soc. Am. Spec. Pap. 350, 181–193.
Jiang, N., Guo, J.H., Zhai, M.G., Zhang, S.Q., 2010. ~2.7 Ga crust growth in the North China craton. Precambrian Res. 179, 37–49.
Jiao, W.F., Wu, Y.B., Yang, S.H., Peng, M., Wang, J., 2009. The oldest basement rock in the Yangtze Craton revealed by zircon U–Pb age and Hf isotope composition. Sci. China Ser. D: Earth Sci. 52, 1393–1399.
Johnson, T.E., Brown, M., Kaus, B.J.P., VanTongeren, J.A., 2014. Delamination and recycling of Archaean crust caused by gravitational instabilities. Nat. Geosci. 7, 47–52.
Jones, R.E., Kirstein, L.A., Kasemann, S.A., Dhuime, B., Elliott, T., Litvak, V.D., Alonso, R., Hinton, R., 2015. Geodynamic controls on the contamination of Cenozoic arc magmas in the southern Central Andes: insights from the O and Hf isotopic composition of zircon. Geochim. Cosmochim. Acta 164, 386–402.
Kemp, A.I.S., Hawkesworth, C.J., Foster, G.L., Paterson, B.A., Woodhead, J.D., Hergt, J.M., Gray, C.M., Whitehouse, M.J., 2007. Magmatic and crustal differentiation history of granitic rocks from Hf–O isotopes in zircon. Science 315, 980–983.
Kemp, A.I.S., Hawkesworth, C.J., Paterson, B.A., Foster, G.L., Kinny, P.D., Whitehouse, M.J., Maas, R., 2006. Exploring the plutonic–volcanic link: a zircon U–Pb, Lu–Hf and O isotope study of paired volcanic and granitic units from southeastern Australia. Trans. R. Soc. Edinb. Earth Sci. 97, 337–355.
Korhonen, F.J., Johnson, S.P., 2015. The role of radiogenic heat in prolonged intraplate reworking: the Capricorn Orogen explained? Earth Planet. Sci. Lett. 428, 22–32.
Kröner, A., Hoffmann, J.E., Xie, H.Q., Münker, C., Hegner, E., Wan, Y.S., Hofmann, A., Liu, D.Y., Yang, J.H., 2014. Generation of early Archaean grey gneisses through melting of older crust in the eastern Kaapvaal craton, southern Africa. Precambrian Res. 255, 823–846.
Kramers, J.D., Mouri, H., 2011. The geochronology of the Limpopo Complex: a controversy solved. Geol. Soc. Am. Mem. 207, 85–106.
Laurent, O., Martin, H., Moyen, J.F., Doucelance, R., 2014. The diversity and evolution of late-Archean granitoids: evidence for the onset of modern-style plate tectonics between 3.0 and 2.5 Ga. Lithos 205, 208–235.
Laurent, O., Paquette, J.-L., Martin, H., Doucelance, R., Moyen, J.-F., 2013. LA-ICP-MS dating of zircons from Meso- and Neoarchean granitoids of the Pietersburg block (South Africa): crustal evolution at the northern margin of the Kaapvaal craton. Precambrian Res. 230, 209–226.
Li, L.M., Lin, S.F., Davis, D.W., Xiao, W.J., Xing, G.F., Yin, C.Q., 2014. Geochronology and geochemistry of igneous rocks from the Kongling terrane: implications for Mesoarchean to Paleoproterozoic crustal evolution of the Yangtze Block. Precambrian Res. 255, 30–47.
Li, X.H., Li, W.X., Li, Z.X., Lo, C.H., Wang, J., Ye, M.F., Yang, Y.H., 2009. Amalgamation between the Yangtze and Cathaysia Blocks in South China: constraints from SHRIMP U–Pb zircon ages, geochemistry and Nd–Hf isotopes of the Shuangxiwu volcanic rocks. Precambrian Res. 174, 117–128.
Li, Z.X., Li, X.H., Chung, S.L., Lo, C.H., Xu, X., Li, W.X., 2012. Magmatic switch-on and switch-off along the South China continental margin since the Permian: transition from an Andean-type to a Western Pacific-type plate boundary. Tectonophysics 532–535, 271–290.
Ling, W.L., Gao, S., Cheng, J.P., Jiang, L.S., Yuan, H.L., Hu, Z.C., 2006. Neoproterozoic magmatic events within the Yangtze continental interior and along its northern margin and their tectonic implication: constraint from the ELA-ICPMS U–Pb geochronology of zircons from the Mangling and Hannan complexes. Acta Petrol. Sin. 22, 387–396.
Ling, W.L., Gao, S., Zheng, H.F., Zhou, L., Zhao, Z.B., 1998. An Sm–Nd isotopic dating study of the Archean Kongling complex in the Huangling area of the Yangtze craton. Chin. Sci. Bull. 43, 1187–1191.
Liou, J.G., Ernst, W.G., Zhang, R.Y., Tsujimori, T., Jahn, B.M., 2009. Ultrahigh-pressure minerals and metamorphic terranes – the view from China. J. Asian Earth Sci. 35, 199–231.
Liu, D.Y., Nutman, A.P., Compston, W., Wu, J.S., Shen, Q.H., 1992. Remnants of ≥3800 Ma crust in the Chinese part of the Sino-Korean craton. Geology 20, 339–342.
Liu, X.M., Gao, S., Diwu, C.R., Ling, W.L., 2008. Precambrian crustal growth of Yangtze Craton as revealed by detrital zircon studies. Am. J. Sci. 308, 421–468.
Liu, Y.S., Gao, S., Hu, Z.C., Gao, C.G., Zong, K.Q., Wang, D.B., 2010. Continental and oceanic crust recycling-induced melt–peridotite interactions in the Trans-North China Orogen: U–Pb dating, Hf isotopes and trace elements in zircons from mantle xenoliths. J. Petrol. 51, 537–571.
Liu, Y.S., Hu, Z.C., Gao, S., Günther, D., Xu, J., Gao, C.G., Chen, H.H., 2008. In situ analysis of major and trace elements of anhydrous minerals by LA-ICP-MS without applying an internal standard. Chem. Geol. 257, 34–43.
Ludwig, K.R., 2012. User's Manual for Isoplot 3.75: A Geochronological Toolkit for Microsoft Excel. Berkeley Geochronology Center Special Publication, Berkeley, pp. 1–75.
Ma, D.Q., Li, Z.C., Xiao, Z.F., 1997. The constitute, geochronology and geologic evolution of the Kongling Complex, western Hubei. Acta Geol. Sin. 18, 233–241.
Maniar, P.D., Piccoli, P.M., 1989. Tectonic discrimination of granitoids. Geol. Soc. Am. Bull. 101, 635–643.
Manikyamba, C., Kerrich, R., 2012. Eastern Dharwar Craton, India: continental lithosphere growth by accretion of diverse plume and arc terranes. Geosci. Front. 3, 225–240.
Martin, H., 1993. The mechanisms of petrogenesis of the Archaean continental crust – comparison with modern processes. Lithos 30, 373–388.
Martin, H., 1994. The Archean grey gneisses and the genesis of continental crust. In: Condie, K.C. (Ed.), Developments in Precambrian Geology. Elsevier, Amsterdam, pp. 205–259 (Chapter 6).
Martin, H., Moyen, J.-F., 2002. Secular changes in tonalite-trondhjemite-granodiorite composition as markers of the progressive cooling of Earth. Geology 30, 319–322.
Martin, H., Moyen, J.-F., Guitreau, M., Blichert-Toft, J., Le Pennec, J.-L., 2014. Why Archaean TTG cannot be generated by MORB melting in subduction zones. Lithos 198–199, 1–13.
Martin, H., Smithies, R.H., Rapp, R., Moyen, J.F., Champion, D., 2005. An overview of adakite, tonalite–trondhjemite–granodiorite (TTG), and sanukitoid: relationships and some implications for crustal evolution. Lithos 79, 1–24.
McDonough, W.F., Sun, S.S., 1995. The composition of the Earth. Chem. Geol. 120, 223–253.
McLoughlin, N., Grosch, E.G., Kilburn, M.R., Wacey, D., 2012. Sulfur isotope evidence for a Paleoarchean subseafloor biosphere, Barberton, South Africa. Geology 40, 1031–1034.
Mojzsis, S.J., Arrhenius, G., McKeegan, K.D., Harrison, T.M., Nutman, A.P., Friend, C.R.L., 1996. Evidence for life on Earth before 3,800 million years ago. Nature 384, 55–59.
Moyen, J.-F., 2011. The composite Archaean grey gneisses: petrological significance, and evidence for a non-unique tectonic setting for Archaean crustal growth. Lithos 123, 21–36.
Moyen, J.-F., Martin, H., 2012. Forty years of TTG research. Lithos 148, 312–336.
Moyen, J.F., Martin, H., Jayananda, M., Auvray, B., 2003. Late Archaean granites: a typology based on the Dharwar Craton (India). Precambrian Res. 127, 103–123.
Nicholls, I.A., Harris, K.L., 1980. Experimental rare earth element partition coefficients for garnet, clinopyroxene and amphibole coexisting with andesitic and basaltic liquids. Geochim. Cosmochim. Acta 44, 287–308.
Nutman, A.P., McGregor, V.R., Friend, C.R.L., Bennett, V.C., Kinny, P.D., 1996. The Itsaq Gneiss Complex of southern West Greenland; the world's most extensive record of early crustal evolution (3900–3600 Ma). Precambrian Res. 78, 1–39.
Paces, J.B., Miller, J.D., 1993. Precise U–Pb ages of Duluth Complex and related mafic intrusions, northeastern Minnesota: geochronological insights to physical, petrogenetic, paleomagnetic, and tectonomagmatic processes associated with the 1.1 Ga Midcontinent Rift System. J. Geophys. Res. Solid Earth 98, 13997–14013.
Patchett, P.J., Tatsumoto, M., 1980. A routine high-precision method for Lu–Hf isotope geochemistry and chronology. Contrib. Mineral. Petrol. 75, 263–267.
Pehrsson, S.J., Berman, R.G., Eglington, B., Rainbird, R., 2013. Two Neoarchean supercontinents revisited: the case for a Rae family of cratons. Precambrian Res. 232, 27–43.
Peng, M., Wu, Y.B., Gao, S., Zhang, H.F., Wang, J., Liu, X.C., Gong, H.J., Zhou, L., Hu, Z.C., Liu, Y.S., Yuan, H.L., 2012. Geochemistry, zircon U–Pb age and Hf isotope compositions of Paleoproterozoic aluminous A-type granites from the Kongling terrain, Yangtze Block: constraints on petrogenesis and geologic implications. Gondwana Res. 22, 140–151.
Peng, M., Wu, Y.B., Wang, J., Jiao, W.F., Liu, X.C., Yang, S.H., 2009. Paleoproterozoic mafic dyke from Kongling terrain in the Yangtze Craton and its implication. Chin. Sci. Bull. 54, 1098–1104.
Polat, A., Kerrich, R., 2002. Nd-isotope systematics of ~2.7 Ga adakites, magnesian andesites, and arc basalts, Superior Province: evidence for shallow crustal recycling at Archean subduction zones. Earth Planet. Sci. Lett. 202, 345–360.
Polat, A., Kerrich, R., Wyman, D.A., 1998. The late Archean Schreiber–Hemlo and White River–Dayohessarah greenstone belts, Superior Province: collages of oceanic plateaus, oceanic arcs, and subduction–accretion complexes. Tectonophysics 289, 295–326.
Qiu, Y.M., Gao, S., McNaughton, N.J., Groves, D.I., Ling, W.L., 2000. First evidence of >3.2 Ga continental crust in the Yangtze craton of south China and its implications for Archean crustal evolution and Phanerozoic tectonics. Geology 28, 11–14.
Rämö, O.T., Halla, J., Nironen, M., Lauri, L.S., Kurhila, M.I., Käpyaho, A., Sorjonen-Ward, P., Äikäs, O.,2005. EUROGRANITES 2005 – Proterozoic and Archean granites and related rocks of the Finnish Precambrian. In: Eurogranites 2005 Field Conference. Publications of the Department of Geology, p. 130.
Rey, P.F., Coltice, N., Flament, N., 2014. Spreading continents kick-started plate tectonics. Nature 513, 405–408.
Rudnick, R.L., Gao, S., Ling, W.L., Liu, Y.S., McDonough, W.F., 2004. Petrology and geochemistry of spinel peridotite xenoliths from Hannuoba and Qixia, North China craton. Lithos 77, 609–637.

Söderlund, U., Patchett, P.J., Vervoort, J.D., Isachsen, C.E., 2004. The ^{176}Lu decay constant determined by Lu–Hf and U–Pb isotope systematics of Precambrian mafic intrusions. Earth Planet. Sci. Lett. 219, 311–324.
Said, N., Kerrich, R., Groves, D., 2010. Geochemical systematics of basalts of the Lower Basalt Unit, 2.7 Ga Kambalda Sequence, Yilgarn craton, Australia: plume impingement at a rifted craton margin. Lithos 115, 82–100.
Schaltegger, U., Zeilinger, G., Frank, M., Burg, J.-P., 2002. Multiple mantle sources during island arc magmatism: U–Pb and Hf isotopic evidence from the Kohistan arc complex, Pakistan. Terra Nova 14, 461–468.
Schopf, J.W., 1993. Microfossils of the Early Archean Apex chert: new evidence of the antiquity of life. Science 260, 640–646.
Shirey, S.B., Richardson, S.H., 2011. Start of the Wilson cycle at 3 Ga shown by diamonds from subcontinental mantle. Science 333, 434–436.
Sisson, T.W., 1994. Hornblende-melt trace-element partitioning measured by ion microprobe. Chem. Geol. 117, 331–344.
Sisson, T.W., Ratajeski, K., Hankins, W.B., Glazner, A.F., 2005. Voluminous granitic magmas from common basaltic sources. Contrib. Mineral. Petrol. 148, 635–661.
Smithies, R.H., 2000. The Archaean tonalite–trondhjemite–granodiorite (TTG) series is not an analogue of Cenozoic adakite. Earth Planet. Sci. Lett. 182, 115–125.
Smithies, R.H., Champion, D.C., 2000. The Archaean high-Mg diorite suite: links to tonalite–trondhjemite–granodiorite magmatism and implications for early Archaean crustal growth. J. Petrol. 41, 1653–1671.
Song, B., Nutman, A.P., Liu, D.Y., Wu, J.S., 1996. 3800 to 2500 Ma crustal evolution in the Anshan area of Liaoning Province, northeastern China. Precambrian Res. 78, 79–94.
Staudigel, H., Furnes, H., DeWit, M., 2015. Paleoarchean trace fossils in altered volcanic glass. Proc. Natl. Acad. Sci. 112, 6892–6897.
Sun, M., Chen, N.S., Zhao, G.C., Wilde, S.A., Ye, K., Guo, J.H., Chen, Y., Yuan, C., 2008. U–Pb zircon and Sm–Nd isotopic study of the Huangtuling granulite, Dabie-Sulu Belt, China: implication for the Paleoproterozoic tectonic history of the Yangtze Craton. Am. J. Sci. 308, 469–483.
Tang, M., Wang, X.L., Shu, X.J., Wang, D., Yang, T., Gopon, P., 2014. Hafnium isotopic heterogeneity in zircons from granitic rocks: geochemical evaluation and modeling of zircon effect in crustal anatexis. Earth Planet. Sci. Lett. 389, 188–199.
Taylor, S.R., McLennan, S.M., 1985. The Continental Crust: Its Composition and Evolution. Blackwell Scientific Publications, Palo Alto, CA, United States, 312 pp.
Thirlwall, M.F., Anczkiewicz, R., 2004. Multidynamic isotope ratio analysis using MC–ICP–MS and the causes of secular drift in Hf, Nd and Pb isotope ratios. Int. J. Mass spectrom. 235, 59–81.
Van Kranendonk, M.J., Hugh Smithies, R., Hickman, A.H., Champion, D.C., 2007. Review: Secular tectonic evolution of Archean continental crust: interplay between horizontal and vertical processes in the formation of the Pilbara Craton, Australia. Terra Nova 19, 1–38.
Vermeesch, P., 2012. On the visualisation of detrital age distributions. Chem. Geol. 312–313, 190–194.
Wan, Y.S., Liu, D.Y., Nutman, A., Zhou, H.Y., Dong, C.Y., Yin, X.Y., Ma, M.Z., 2012. Multiple 3.8–3.1 Ga tectono-magmatic events in a newly discovered area of ancient rocks (the Shengousi Complex), Anshan, North China Craton. J. Asian Earth Sci. 54–55, 18–30.
Wan, Y.S., Liu, D.Y., Song, B., Wu, J.S., Yang, C.H., Zhang, Z.Q., Geng, Y.S., 2005. Geochemical and Nd isotopic compositions of 3.8 Ga meta-quartz dioritic and trondhjemitic rocks from the Anshan area and their geological significance. J. Asian Earth Sci. 24, 563–575.
Wan, Y.S., Xie, S.W., Yang, C.H., Kröner, A., Ma, M.Z., Dong, C.Y., Du, L.L., Xie, H.Q., Liu, D.Y., 2014. Early Neoarchean (~2.7 Ga) tectono-thermal events in the North China Craton: a synthesis. Precambrian Res. 247, 45–63.
Wang, C.Y., Campbell, I.H., Stepanov, A.S., Allen, C.M., Burtsev, I.N., 2011. Growth rate of the preserved continental crust: II. Constraints from Hf and O isotopes in detrital zircons from Greater Russian Rivers. Geochim. Cosmochim. Acta 75, 1308–1345.
Wang, L.J., Griffin, W.L., Yu, J.H., O'Reilly, S.Y., 2013. U–Pb and Lu–Hf isotopes in detrital zircon from Neoproterozoic sedimentary rocks in the northern Yangtze Block: implications for Precambrian crustal evolution. Gondwana Res. 23, 1261–1272.
Wang, Z.J., Wang, J., Du, Q.D., Deng, Q., Yang, F., 2013a. The evolution of the Central Yangtze Block during early Neoarchean time: evidence from geochronology and geochemistry. J. Asian Earth Sci. 77, 31–44.
Wang, Z.J., Wang, J., Du, Q.D., Deng, Q., Yang, F., Wu, H., 2013b. Mature Archean continental crust in the Yangtze craton: evidence from petrology, geochronology and geochemistry. Chin. Sci. Bull. 58, 2360–2369.
Watkins, J.M., Clemens, J.D., Treloar, P.J., 2007. Archaean TTGs as sources of younger granitic magmas: melting of sodic metatonalites at 0.6–1.2 GPa. Contrib. Mineral. Petrol. 154, 91–110.
Wei, J.Q., Jing, M.M., 2013. Chronology and geochemistry of amphibolites from the Kongling Complex. Chin. J. Geol. 48, 970–983.
Wei, J.Q., Wang, J.X., 2012. Zircon age and Hf isotope compositions of amphibolite enclaves from the Kongling complex. Geol. J. China Univ. 18, 589–600.
Whitney, D.L., Evans, B.W., 2010. Abbreviations for names of rock-forming minerals. Am. Mineral. 95, 185–187.
Wiedenbeck, M., Allé, P., Corfu, F., Griffin, W.L., Meier, M., Oberli, F., Quadt, A.V., Roddick, J.C., Spiegel, W., 1995. Three natural zircon standards for U–Th–Pb, Lu–Hf, trace element and REE analyses. Geostandards Newslett. 19, 1–23.
Wilson, A.H., Shirey, S.B., Carlson, R.W., 2003. Archaean ultra-depleted komatiites formed by hydrous melting of cratonic mantle. Nature 423, 858–861.
Wu, Y.B., Gao, S., Gong, H.J., Xiang, H., Jiao, W.F., Yang, S.H., Liu, Y.S., Yuan, H.L., 2009. Zircon U–Pb age, trace element and Hf isotope composition of Kongling terrane in the Yangtze Craton: refining the timing of Palaeoproterozoic high-grade metamorphism. J. Metamorph. Geol. 27, 461–477.
Wu, Y.B., Zheng, Y.F., 2013. Tectonic evolution of a composite collision orogen: an overview on the Qinling–Tongbai–Hong'an–Dabie–Sulu orogenic belt in central China. Gondwana Res. 23, 1402–1428.
Wu, Y.B., Zheng, Y.F., Gao, S., Jiao, W.F., Liu, Y.S., 2008. Zircon U–Pb age and trace element evidence for Paleoproterozoic granulite-facies metamorphism and Archean crustal rocks in the Dabie Orogen. Lithos 101, 308–322.
Wu, Y.B., Zhou, G.Y., Gao, S., Liu, X.C., Qin, Z.W., Wang, H., Yang, J.Z., Yang, S.H., 2014. Petrogenesis of Neoarchean TTG rocks in the Yangtze Craton and its implication for the formation of Archean TTGs. Precambrian Res. 254, 73–86.
Wyman, D.A., 2003. Upper mantle processes beneath the 2.7 Ga Abitibi belt, Canada: a trace element perspective. Precambrian Res. 127, 143–165.
Xiong, Q., Zheng, J.P., Yu, C.M., Su, Y.P., Tang, H.Y., Zhang, Z.H., 2009. Zircon U–Pb age and Hf isotope of Quanyishang A-type granite in Yichang: signification for the Yangtze continental cratonization in Paleoproterozoic. Chin. Sci. Bull. 54, 436–446.
Yin, C.Q., Lin, S.F., Davis, D.W., Zhao, G.C., Xiao, W.J., Li, L.M., He, Y.H., 2013. 2.1–1.85 Ga tectonic events in the Yangtze Block, South China: petrological and geochronological evidence from the Kongling Complex and implications for the reconstruction of supercontinent Columbia. Lithos 182–183, 200–210.
Zeh, A., Gerdes, A., Klemd, R., Barton, J.M., 2007. Archaean to Proterozoic crustal evolution in the central zone of the Limpopo Belt (South Africa–Botswana): constraints from combined U–Pb and Lu–Hf isotope analyses of zircon. J. Petrol. 48, 1605–1639.
Zeh, A., Gerdes, A., Barton, J.M., 2009. Archean accretion and crustal evolution of the Kalahari Craton – the zircon age and Hf isotope record of granitic rocks from Barberton/Swaziland to the Francistown arc. J. Petrol. 50, 933–966.
Zeh, A., Gerdes, A., Barton Jr., J., Klemd, R., 2010. U–Th–Pb and Lu–Hf systematics of zircon from TTG's, leucosomes, meta-anorthosites and quartzites of the Limpopo Belt (South Africa): constraints for the formation, recycling and metamorphism of Palaeoarchaean crust. Precambrian Res. 179, 50–68.
Zeh, A., Gerdes, A., Millonig, L., 2011. Hafnium isotope record of the Ancient Gneiss Complex, Swaziland, southern Africa: evidence for Archaean crust–mantle formation and crust reworking between 3.66 and 2.73 Ga. J. Geol. Soc. 168, 953–964.
Zeh, A., Stern, R.A., Gerdes, A., 2014. The oldest zircons of Africa – their U–Pb–Hf–O isotope and trace element systematics, and implications for Hadean to Archean crust–mantle evolution. Precambrian Res. 241, 203–230.
Zhai, M.G., Santosh, M., 2011. The early Precambrian odyssey of the North China Craton: a synoptic overview. Gondwana Res. 20, 6–25.
Zhang, R.Y., Liou, J.G., Ernst, W.G., 2009. The Dabie–Sulu continental collision zone: a comprehensive review. Gondwana Res. 16, 1–26.
Zhang, S.B., Zheng, Y.F., Wu, Y.B., Zhao, Z.F., Gao, S., Wu, F.Y., 2006a. Zircon isotope evidence for ≥3.5 Ga continental crust in the Yangtze craton of China. Precambrian Res. 146, 16–34.
Zhang, S.B., Zheng, Y.F., Wu, Y.B., Zhao, Z.F., Gao, S., Wu, F.Y., 2006b. Zircon U–Pb age and Hf–O isotope evidence for Paleoproterozoic metamorphic event in South China. Precambrian Res. 151, 265–288.
Zhang, S.B., Zheng, Y.F., Wu, Y.B., Zhao, Z.F., Gao, S., Wu, F.Y., 2006c. Zircon U–Pb age and Hf isotope evidence for 3.8 Ga crustal remnant and episodic reworking of Archean crust in South China. Earth Planet. Sci. Lett. 252, 56–71.
Zhang, S.B., Zheng, Y.F., Zhao, Z.F., Wu, Y.B., Yuan, H.L., Wu, F.Y., 2008. Neoproterozoic anatexis of Archean lithosphere: geochemical evidence from felsic to mafic intrusions at Xiaofeng in the Yangtze Gorge, South China. Precambrian Res. 163, 210–238.
Zhang, Z.Q., Zhang, G.W., Tang, S., Wang, J.H., 2001. On the age of metamorphic rocks of the Yudongzi Group and the Archean crystalline basement of the Qinling Orogen. Acta Geol. Sin. 775, 198–204.
Zhao, G.C., Cawood, P.A., 2012. Precambrian geology of China. Precambrian Res. 222–223, 13–54.
Zhao, G.C., Cawood, P.A., Wilde, S.A., Sun, M., 2002. Review of global 2.1–1.8 Ga orogens: implications for a pre-Rodinia supercontinent. Earth Sci. Rev. 59, 125–162.
Zhao, G.C., Zhai, M.G., 2013. Lithotectonic elements of Precambrian basement in the North China Craton: review and tectonic implications. Gondwana Res. 23, 1207–1240.
Zhao, J.H., Zhou, M.F., Zheng, J.P., Griffin, W.L., 2013. Neoproterozoic tonalite and trondhjemite in the Huangling complex, South China: crustal growth and reworking in a continental arc environment. Am. J. Sci. 313, 540–583.
Zheng, H.B., Clift, P.D., Wang, P., Tada, R., Jia, J.T., He, M.Y., Jourdan, F., 2013. Pre-Miocene birth of the Yangtze River. Proc. Natl. Acad. Sci. 110, 7556–7561.
Zheng, J.P., Griffin, W.L., O'Reilly, S.Y., Zhang, M., Pearson, N., Pan, Y.M., 2006. Widespread Archean basement beneath the Yangtze craton. Geology 34, 417–420.
Zheng, W.Z., Liu, G.L., Wang, X.W., 1991. A new information of Archaean Eon for the Kongling Group in northern Huangling Anticline, Hubei. Bull. Yichang Inst. Geol. Miner. Resour. CAGS 16, 97–107.
Zhou, G.Y., Wu, Y.B., Gao, S., Yang, J.Z., Zheng, J.P., Qin, Z.W., Wang, H., Yang, S.H., 2015. The 2.65 Ga A-type granite in the northeastern Yangtze craton: petrogenesis and geological implications. Precambrian Res. 258, 247–259.
Zhu, X.Y., Zhai, M.G., Chen, F.K., Lyu, B., Wang, W., Peng, P., Hu, B., 2013. ~2.7-Ga crustal growth in the North China craton: evidence from zircon U–Pb ages and Hf isotopes of the Sushui Complex in the Zhongtiao Terrane. J. Geol. 121, 239–254.